MUSCULOSKELETAL ADAPTATION OF YOUNG AND OLDER ADULTS IN RESPONSE TO ENVIRONMENTAL, PHYSICAL, AND COGNITIVE CONDITIONS

by

Amy E. Holcomb

A thesis

submitted in partial fulfillment

of the requirements for the degree of

Master of Science in Mechanical Engineering

Boise State University

August 2021

© 2021

Amy E. Holcomb

ALL RIGHTS RESERVED

BOISE STATE UNIVERSITY GRADUATE COLLEGE

DEFENSE COMMITTEE AND FINAL READING APPROVALS

of the thesis submitted by

Amy E. Holcomb

Thesis Title: Musculoskeletal Adaptation of Young and Older Adults in Response to Environmental, Physical, and Cognitive Conditions

Date of Final Oral Examination: 21 May 2021

The following individuals read and discussed the dissertation submitted by student Amy E. Holcomb, and they evaluated the student's presentation and response to questions during the final oral examination. They found that the student passed the final oral examination.

Clare K. Fitzpatrick Ph.D.	Chair, Supervisory Committee
Tyler N. Brown Ph.D.	Member, Supervisory Committee
Erin M. Mannen Ph.D.	Member, Supervisory Committee

The final reading approval of the thesis was granted by Clare K. Fitzpatrick Ph.D., Chair of the Supervisory Committee. The thesis was approved by the Graduate College.

DEDICATION

This thesis is dedicated to the One who has given me the opportunity, skills, and community necessary to complete this work.

ACKNOWLEDGMENT

This thesis would not have happened without the help and support of family, friends, lab mates, and the sanity provided through the outdoors. In particular, my thesis advisor, Dr. Clare Fitzpatrick, gave me the attention and support necessary to tackle a Master's in human biomechanics. Dr. Tyler Brown, director of the Center for Orthopaedic Biomechanics Research Laboratory, was invaluable in the experimental data collection process.

ABSTRACT

Accidental falls present a large functional and financial burden among people aged 65 years and older. Falls, injuries associated with falls, and the fear of falling decrease quality of life, physical function, and independence for older adults. To prevent falls, improve stability, and protect joints from damage or injury, the typical response to "challenging" conditions include cautious gait, increase muscle co-contraction, and decreased range of motion. These compensatory strategies are more pronounced in the older adult population with apprehensive "cautious" gait at slower speeds, decreased knee flexion, and increased muscle activation around the knee and ankle. The underlying mechanisms and driving forces behind accidental falls are not well investigated. Additionally, the effects of aging on the ability of the musculoskeletal system to adapt to changing and challenging conditions is poorly understood. There exists a gap in knowledge regarding the relationship between accidental fall risk factors, knee joint stability, adaptation mechanisms, and whole-body function. Establishing these relationships between stability and musculoskeletal adaptation may have far reaching implications on improving whole-body function through targeted joint- and muscle-level interventions.

The purpose of this study was to compare neuromechanics (whole-body function) of young and older adults walking across various external challenging conditions, quantifying adaptation strategies for both cohorts. This was accomplished through

two objectives. In the first objective, joint kinematics, ground reaction force loading and impulse, and lower-limb muscle activation strategies for ten young and ten older adults walking on normal, slick, and uneven surfaces were compared to assess how musculoskeletal adaptation strategies change with age. For the second objective, a pipeline to create subject-specific lower-limb finite element models was developed to investigate joint-level behavior across cohorts. Proof-of-concept for the model development and analysis process was demonstrated for an older and a young adult to implement a novel metric for functional stability and dynamic laxity of the knee joint during the stance phase of gait.

Kinematic, force, and muscle activation analysis showed that an uneven surface reduced sagittal joint kinematics during the first 25% of stance, indicating a surface-specific compensatory strategy. Additionally, older adults tended to prepare for and step onto the uneven surfaces in a more conservative manner with joints more flexed or bent. This anticipatory or cautious musculoskeletal adaptation of older adults was also seen in reduced magnitude of initial vertical loading during the loading response of stance (0-25% stance). Results of this research study provide insight into the differences that exist in joint stiffening and other musculoskeletal adaption strategies for young and older adults during external challenging conditions. Specifically, understanding the relationships between joint-level stability and whole-body musculoskeletal function has the potential to inform targeted muscle training programs and joint-level interventions to improve whole-body musculoskeletal function and reduce risk of injuries.

TABLE OF CONTENTS

LIST OF TABLES

LIST OF FIGURES

LIST OF ABBREVIATIONS

% COCON	Percent Co-contraction
ACL	Anterior Cruciate Ligament
ALL	Anterolateral Ligament
ANOVA	Analysis of Variance
AP	Anteroposterior/Anterior-Posterior
BF	Biceps Femoris
BW	Body Weight
EMG	Electromyography
F1	First Vertical Loading Peak (25% stance)
F2	Vertical Ground Reaction Force Minima
F3	Second Vertical Loading Peak (75% stance)
GL	Gastrocnemius Lateralis
GRF	Ground Reaction Force
HS	Heel Strike (0% stance)
IC	Initial Contact (0% Stance)
ICP	Iterative Closest Points
IE	Internal-External
LCL	Lateral Collateral Ligament
LR	Loading Response (0-25% stance)

MCL	Medial Collateral Ligament
ML	Mediolateral/Medial-Lateral
MRI	Magnetic Resonance Imaging
OA	Older Adults
PCAP	Posterior Capsule
PCL	Posterior Cruciate Ligament
PFL	Popliteal Fibular Ligament
PL	Patellar Ligament
POL	Posterior Oblique Ligament
Q:H	Quadricep-to-Hamstring Ratio
RF	Rectus Femoris
ROM	Range of Motion
SI	Superoinferior/Superior-Inferior
SM	Semimembranosus
TA	Tibialis Anterior
TF	Tibiofemoral
TO	Toe Off (100% stance)
VV	Varus-Valgus
VL	Vastus Lateralis
VM	Vastus Medialis
YA	Young Adults

CHAPTER 1:

INTRODUCTION

1.1 Motivation

The main motivation for this research study is the prevalence of accidental falls in the older adult population. Accidental falls present a large functional and financial burden among people aged 65 years and older. Thirty-six million older adults fall each year costing $34 billion in the US annually with one in five falls resulting in injury and 27,000 deaths (Homer *et al.*, 2017). The single most common injury from falls in older adults is hip fractures resulting in at least 300,000 hospitalizations. 30% of falls occur during a standing turning movement or while bending, leading to lateral fall and increased risk of hip fracture (HCUPnet, 2012; Moreland *et al.*, 2020). Hip fractures are associated with significant morbidity and mortality within this population, increasing the likelihood of death 5-fold for older women and 8-fold for older men in the first three months after injury (Schnell *et al.*, 2010).

Risk of accidental falls increases with age. One in three adults over the age of 65 will experience an accidental fall. This increases to one in two adults over the age of 80 (Ambrose *et al.*, 2013). With aging, muscles naturally get weaker and people will tend to decrease some activities while avoiding others, contributing to muscle weakness and poor balance. Risk factors are also psychological and environmental (Rubenstein &

Josephson, 2002; Nevitt *et al.*, 2016). Fifty percent (50%) of older adults who have previously fallen are afraid of falling again, compared to approximately one quarter (27%) of their peers who have not had a previous fall (Hallal *et al.*, 2013). Of those who have fallen once, almost half become recurrent fallers and will fall again within the next year (Berry & Miller, 2008). Falls commonly experienced by older adults also include slipping, on wet or slick surfaces, or tripping, on uneven surfaces, or at the transition between surfaces (Berry & Miller, 2008; Alcock *et al.*, 2016; Allin *et al.*, 2016). Another risk factor for accidental falls is knee joint stability. Knee instability, identified as knee buckling or giving way, or slippage of the knee without buckling, results in a 4.5-fold increase in risk of recurrent falls (Nevitt *et al.*, 2016).

The typical response to changes in external conditions or a "challenging" surface is a cautious gait or shortened stride length, increased muscle activation, and decreased range of motion to improve stability and protect joints from damage or injury. Shorter stride length brings the center of mass closer to the leading foot, increasing stability during gait (Espy *et al.*, 2010). Co-contraction around the knee increases tibiofemoral stability, protecting the cruciate ligaments (Li *et al.*, 1999; Hallal *et al.*, 2013). However, excessive co-contraction increases metabolic cost leading to fatigue, which in turn leads to decreased ability to provide adequate joint stability, thus increasing the risk of falling. Additionally, increased co-contraction can result in excessive loading and wear of the cartilage, contributing to the development and progression of osteoarthritis.

Compensatory strategies during challenging conditions are more pronounced in older adult populations with cautious slower walking speeds, increased muscle co-activation around the knee and ankle, and decreased knee flexion, compared to

younger adults (Saywell *et al.*, 2012; Hallal *et al.*, 2013; Lee *et al.*, 2017). The presence of an uneven surface has been shown to increase knee flexion for older adults, compared to young adults, while increasing hip flexion and decreasing ankle dorsiflexion regardless of age (Dixon *et al.*, 2018). For a step-down activity, older adults exhibit decreased knee flexion and increased muscle activity of the quadriceps, compared to young adults (Saywell *et al.*, 2012).

Reduction in muscle strength, such as that observed with increasing age, impacts the attenuation of impulse during the initial loading response of weight acceptance during activities of daily living, thus increasing the risk of joint damage, contributing to the onset and development of osteoarthritis. Knee flexion has previously been identified as important in the attenuation of impulse during the loading response of stance (Saywell *et al.*, 2012). The development of knee osteoarthritis has been found to be associated with reduced knee flexion during early stance (Hinman *et al.*, 2002). To compensate for weaker muscles, older adults employ higher muscle activity and rates of co-contraction of muscles around the knee to stiffen the joint and improve stability. Increased co-contraction leads to increased potential for fatigue during gait and may increase risk for falls (Hahn *et al.*, 2005). Specific muscle activation strategies vary across phases of gait (Schmitz *et al.*, 2009). For example, older adults were found to have higher activation of quadriceps (vastus lateralis and medialis) during the loading response portion of stance and increased shank muscle activation during mid-stance, compared to younger adults (Schmitz *et al.*, 2009).

In previous studies investigating changes during activities of daily life, the emphasis has been on specific age or sex groups, or specific metrics, activities, or conditions. Many researchers have focused on spatiotemporal metrics of gait, such as step width,

step length, and velocity (Grabiner *et al.*, 2001; Owings & Grabiner, 2004; Thies *et al.*, 2005; Schmitz *et al.*, 2009; Worsley *et al.*, 2011; Dixon *et al.*, 2018). Studies that investigated age-related changes in muscle activity often did not examine metrics representative of whole-body physiological function, such as joint kinematics (Schmitz *et al.*, 2009). While musculoskeletal differences have been frequently reported between young and older adults, few studies to date have combined kinematics, kinetics, and muscle activation for young and older adult groups to assess musculoskeletal adaptation during gait due to changing surface conditions or increasing age.

1.2 Research Goals

The risk of accidental falls is complex and multifaceted. Studies have investigated the whole-body level response, such as spatiotemporal metrics of gait, for different external conditions to establish these fall predictors. However, the underlying musculoskeletal mechanisms and driving forces behind accidental falls, as well as the effects of aging on the ability of the musculoskeletal system to adapt are poorly understood. Establishing the relationships between accidental fall risk factors, knee joint stability, adaptation mechanisms, and musculoskeletal neuromechanics may have far reaching implications on improving whole-body function through targeted joint- and muscle-level interventions.

The purpose of this study is to compare neuromechanics (whole-body function) of young and older adults walking across various challenging external conditions, quantifying adaptation strategies for both cohorts. Specifically, joint kinematics, ground reaction forces, and electromyography activity during the stance phase of challenging gait were calculated and compared within each cohort to a baseline condition as well as compared between age groups.

We hypothesize that challenging conditions will reduce lower limb range of motion for both young and older adults but with larger reduction and different compensatory strategies employed by older adults. Specifically, older adults will compensate for challenging conditions with decreased knee flexion range of motion and increased muscle co-contraction around the knee. This co-contraction will result in increased impulse during the loading response of stance phase as the weaker muscles are less able to attenuate impulse, resulting in reduced knee joint stability. These differences in experimental whole-body neuromechanics will translate to increased dynamic knee laxity, simulated computationally, at the joint-level during some portions of gait due to muscle weakness but reduced laxity at other times during gait because of increased co-activation of muscles around the knee joint and more cautious flexion angles.

The primary aims of this thesis work are:

- **AIM 1: Evaluate musculoskeletal adaptation during gait on challenging surfaces between young and older adults**

Joint kinematics, vertical loading, breaking and propulsive impulse, and quadriceps and hamstrings activation strategies were investigated for young and older adults walking on challenging surfaces to assess musculoskeletal adaptation strategies to environmental challenges across ages.

- **AIM 2: Develop subject-specific finite element models capable of estimating joint-level differences in stability and adaptation strategies for different age groups**

Subject-specific finite element simulations were developed and applied as proof-of-concept of a novel metric for functional, dynamic knee stability for participants from

young and older adult cohorts.

The long-term objective of this work is to quantify the relationship between knee stability and whole-body neuromechanics. This will allow us to identify targeted interventions that may reduce the risk of falls in an aging population. Working towards this objective, the goals of this thesis are to understand the differences in musculoskeletal response to challenging conditions between young and older adults during challenging gait and to develop a computational method to predict subject-specific joint level stability in the knee.

CHAPTER 2:

MANUSCRIPT "MUSCULOSKELETAL ADAPTATION OF YOUNG AND OLDER ADULTS IN RESPONSE TO CHALLENGING SURFACE CONDITIONS"

The following manuscript will be submitted to the Journal of Biomechanics.

2.1 Introduction

Accidental falls present a large functional and financial burden among people aged 65 years and older. One in three adults over the age of 65 will experience an accidental fall. This increases to one in two adults over the age of 80 (Ambrose *et al.*, 2013; Homer *et al.*, 2017). Falls, injuries associated with falls, and fear of falling decrease quality of life, physical function, and independence for older adults (Berry & Miller, 2008; Hallal *et al.*, 2013).

Environmental hazards, such as slick or uneven surfaces, are additional risk factors for accidental falls. Falls commonly experienced by older adults include slipping (wet or slick) or tripping (uneven surface) (Berry & Miller, 2008; Alcock *et al.*, 2016; Allin *et al.*, 2016). The typical response to a "challenging" surface is a shortened stride and increased muscle activation to improve stability and protect joints from

damage or injury. Co-contraction of the quadricep and hamstring muscle groups increases tibiofemoral stability, reducing tibiofemoral motion and protecting the cruciate ligaments from damage (Hallal *et al.*, 2013; Li *et al.*, 1999). However, excessive co-contraction increases the metabolic cost of walking leading to fatigue and increased risk of falling (Hahn *et al.*, 2005; Lee *et al.*, 2017). Compensatory strategies are more pronounced in the older adult population: apprehensive "cautious" gait at slower speeds, decreased knee flexion, and greater muscle co-activation (Hallal *et al.*, 2013; Saywell *et al.*, 2012). Weaker muscles in older adults result in higher muscular demands and rates of co-contraction, leading to increased potential for fatigue during activity of daily living and may increase risk for falls (Hahn *et al.*, 2005).

Reduction in muscle strength observed with increasing age impacts the attenuation of impulse during the initial loading response of weight acceptance during activities of daily living, thus increasing the risk of joint damage, contributing to the onset and development of osteoarthritis. Knee flexion has previously been identified as important in the attenuation of impulse during the loading response of stance (Saywell *et al.*, 2012). Additionally, to compensate for weaker muscles, older adults employ higher muscle activity and rates of co-contraction of muscles around the knee to stiffen the joint and improve stability. Muscle co-contraction has been found to increase with age, with specific muscle activation strategies varying across phases of gait (Schmitz *et al.*, 2009). For example, older adults were found to have higher activation of vastus lateralis and medialis during the loading response portion of stance and increased shank muscle activity during mid-stance, compared to younger adults (Schmitz *et al.*, 2009).

In previous studies investigating changes during activities of daily life, the empha-

sis has been on specific age or sex groups, or specific metrics, activities, or conditions. Many researchers have focused on spatiotemporal metrics of gait, such as step width, step length, and velocity (Grabiner *et al.*, 2001; Owings & Grabiner, 2004; Thies *et al.*, 2005; Schmitz *et al.*, 2009; Worsley *et al.*, 2011; Arnold *et al.*, 2010; Dixon *et al.*, 2018). Studies that investigated age-related changes in muscle activity often did not examine metrics representative of whole-body physiological function, such as joint kinematics (Schmitz *et al.*, 2009).

The presence of an uneven surface has been shown to increase knee flexion for older adults, compared to young adults, while increasing hip flexion and decreasing ankle dorsiflexion regardless of age (Dixon *et al.*, 2018). For a step-down activity, older adults exhibit decreased knee flexion and increased muscle activity of the quadriceps, compared to young adults (Saywell *et al.*, 2012). Few studies to date have combined kinematics, kinetics, and muscle activation for young and older adult groups to assess musculoskeletal adaptation during gait due to changing surfaces or increasing age. The underlying musculoskeletal mechanisms and driving forces behind accidental falls, as well as the effects of aging on the ability of the musculoskeletal system to adapt are poorly understood.

The aims of this study were to (1) compare neuromechanics of young and older adults walking across a variety of challenging surfaces, (2) quantify adaptation strategies, and (3) assess how these musculoskeletal adaptation strategies change with age. We hypothesized that (1) young and older adults will have similar baseline neuromechanics metrics, but challenging surfaces will (2) increase sagittal plane kinematics, (3) increase impulse during loading, and (4) increase muscle activation and co-contraction strategies.

2.2 Methods

Participants

Ten older participants (five male) over the age of 65 and ten active younger (18-25 years old) participants (five male) were recruited according to a protocol approved by Boise State University's Institutional Review Board. Younger participants were recruited from the Boise State population whereas older adult participants were predominantly recruited from the Osher Lifelong Learning Institute for adults over the age of 50. Inclusion criteria were no history of lower extremity or back surgery, no current pain or injury to lower extremity or back in the past six months, and no known neurological disorders. To be included in the older cohort, participants must have also experienced at least one accidental fall in the past 12 months. Participants of diverse height and weight, and representative of diverse ethnicities (Table A.1), were matched across cohorts according to sex, height, and BMI (Table 2.1).

Table 2.1: Participant characteristics

	Young Adults ($n = 10$)	Older Adults ($n = 10$)	p-value
Age (year)	21.60 ± 2.27	69.60 ± 3.17	**<0.001***
Height (cm)	174.10 ± 9.80	171.70 ± 12.90	p=0.64
Weight (kg)	75.61 ± 13.96	74.16 ± 17.33	p=0.84
Speed (ms^{-1})	1.06 ± 0.09	1.02 ± 0.16	p=0.51

*p<0.05. Significant differences between young and older adults.

Data Collection Procedure

Each participant attended the biomechanics laboratory, located in the Center for Orthopaedic and Biomechanics Research, for two data collection sessions: an orientation and isometric strength testing session, followed by a dynamic activity session. During the first session, maximal muscle force production was estimated using a Hu-

mac Norm dynamometer. Torque required for hip, knee, and ankle flexion/extension activities were recorded for each participant's dominant leg. The participant performed hip flexion/extension in a standing pose with target leg moved to 15° flexion. Knee flexion/extension was performed in a seated position with target shank moved to 60° flexion. The participant was prone with ankle held at 0° for the ankle plantar-/dorsi-flexion tests. Three sets of isometric tests were collected for each activity with verbal coaching provided to encourage maximal effort. The overall maximum for each test was used as an upper bound representative of the participant's strength for the relevant muscle group (Tables B.1 - B.2).

During the second biomechanics session, the experimental area consisted of a 10m walkway with two square (45cm x 45cm) surface plates placed at the end of the walkway. Modular floor sections with differing surface conditions (normal, slick, uneven) were constructed to sit on top of in-ground force plates (strain-gauge (AMTI) and piezoelectric (Kistler)). These surfaces could be easily removed and replaced to change the surface conditions. For the slick surface, silk booties were placed over the participant's shoes to augment the low friction condition. From in-house testing, the coefficient of static friction for silk booties on the slick surface was estimated to be $\mu = 0.19$, which is comparable to $\mu = 0.1$ for that of shoes on ice (College, 2012). The uneven surface was composed of 9 smaller squares of differing profile heights within the main surface plate (Figure 2.1). Participants were instructed to walk to the end of the walkway at a self-selected walking speed. The order of surfaces was randomized for each participant using a Latin Square Design. Three walk trials at this preferred speed where the dominant limb contacted the force plate under the first surface were collected for normal (baseline) and challenging surfaces (uneven

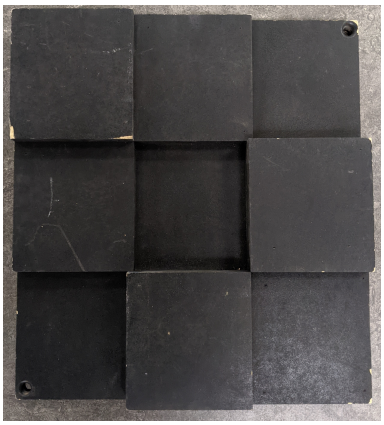

Figure 2.1: Experimental uneven surface plate (45cm x 45cm).

and slick). All participants were attached via safety harness during data collection. Shoe type was self-selected; participants were instructed to wear comfortable, well-fitting tennis shoes or workout shoes (low ankle) for the second biomechanics session. Experimental setup, along with collected metrics and an outline of processing, for an uneven gait trial can be seen in Figure 2.2.

Synchronized ground reaction force, kinematic, and electromyographic data for each study task were collected, processed, and analyzed. Force plate data were used to investigate ground reaction forces and loading impulses. Marker trajectories were used to calculate joint angles. Muscle activation recorded by lower limb surface electrodes were used to estimate percent co-contraction between muscle groups.

Following the second biomechanics session for subject-specific geometry, participants underwent supine 3T magnetic resonance imaging with 1mm slice thickness and 0.2188mm in-plane resolution of the knee joint at a nearby imaging center.

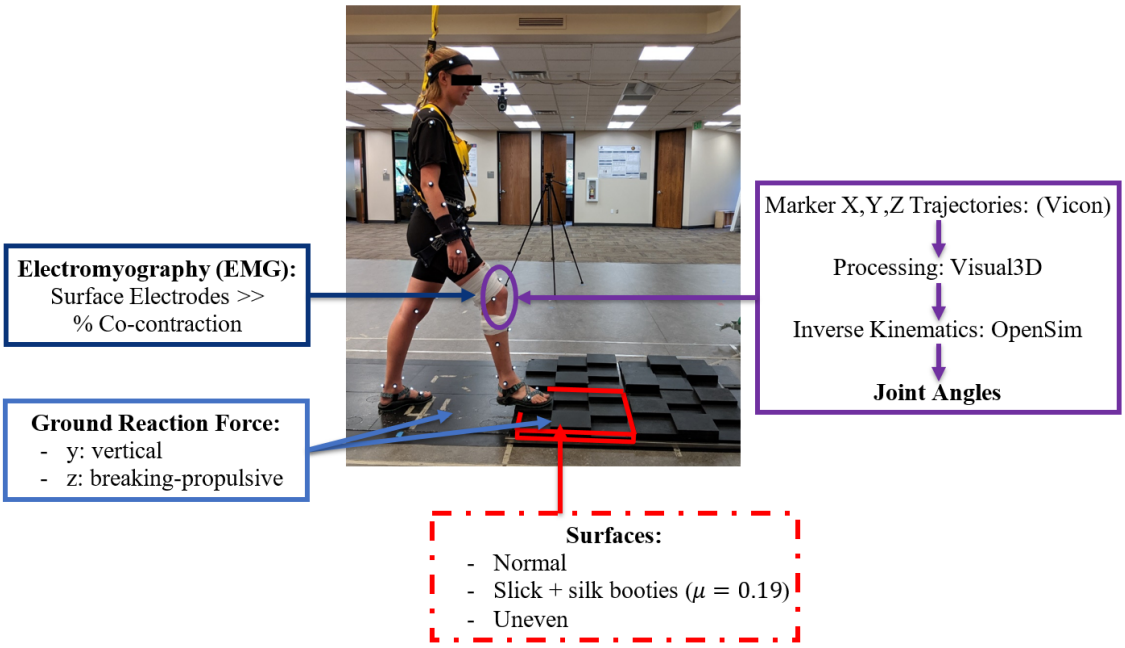

Figure 2.2: Experimental setup for gait on the uneven surface. Safety harness can be seen as the yellow straps across the torso as well as the tether behind the participant's head, connecting the participant to the gantry above (not shown).

Kinetic Data

Ground reaction force (GRF) data were collected in Vicon Nexus (Vicon Nexus 2.10.1, Vicon Motion Systems Ltd., UK) at 240Hz using two strain-gauge (AMTI) and two piezoelectric (Kistler) six-component force platforms embedded in the laboratory floor. GRF data from Vicon was processed in Visual3D using a fourth order low pass Butterworth filter with 12Hz cutoff frequency. Stance phase was identified by the period of each trial where GRF data were recorded for the dominant limb. This length of time was used to identify the relevant portion of kinematic and electromyographic data. Stance phase GRF was time normalized to 101 points and amplitude normalized to participant body weight (BW).

Magnitude (% BW) of peaks were found for the anteroposterior or propulsive-breaking and vertical components of the GRF. Rate of initial vertical loading, as defined by first loading peak (% BW) divided by time to this peak (s), as well as impulse, defined by the area under the force-time curve, for each component during stance phase were also calculated, integrating the GRF across stance phase using Python (Python 3.7). First and second vertical loading peaks were identified as indicated in Figure 2.3.

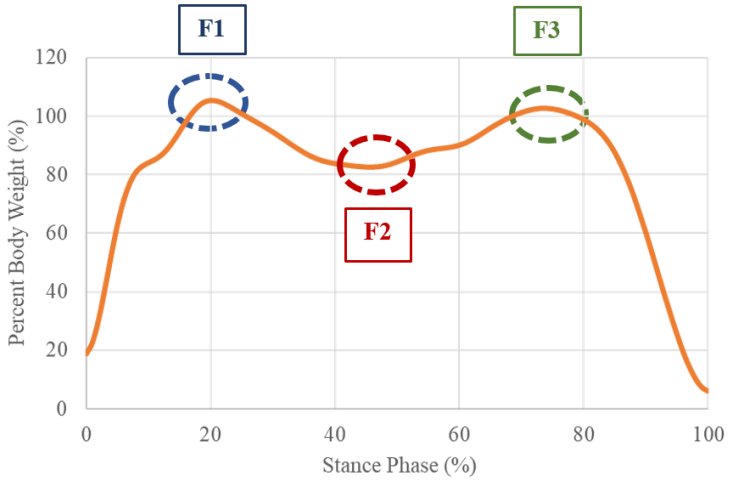

Figure 2.3: Loading peaks from vertical ground reaction force. F1: first peak, F2: local minima between F1 and F3, and F3: second peak.

Kinematic Data

A ten-camera, video-based motion capture system (Vicon Nexus 2.10.1) tracked skin-based retroreflective spherical markers recorded at 240Hz. The following augmented lower body marker set was used to track body segment motions: bilateral anterior superior iliac spine, posterior superior iliac spine, iliac crest, greater trochanter, thigh, medial and lateral epicondyle, proximal, lateral, and distal shank, medial and lateral malleoli, first and fifth metatarsal head, heel, acromion, shoulder, medial and

lateral elbow, lateral forearm, medial and lateral wrist, and hand; four head markers; digital trunk (manubrium and xyphoid process) and back (C7 and T10) markers. The location of the functional hips was calculated using the Gilette algorithm from specific movement trials for each hip in which the joint has modest range of motion about all three axes of rotation (Schwartz & Rozumalski, 2005; C-motion, 2020b).

Marker trajectories from Vicon were filtered in Visual3D (C-Motion, Rockville, MD) to remove noise using a Butterworth, fourth order low pass filter with cutoff frequency of 12 Hz and stance phase was time normalized to percent stance (101 points).

Open source software OpenSim was used to create subject-specific dynamic musculoskeletal models from the experimental marker and GRF data. A generic lower limb and torso OpenSim model with 23 degrees of freedom and 92 musculotendon actuators (gait2392_simbody.osim) was scaled using the static pose marker data for each experimental participant (Delp *et al.*, 2007). Pairs of experimental and model markers were compared to determine scaling factors, which were utilized to scale the generic OpenSim model to create a subject-specific model for each participant. This scaled model was submitted with marker trajectories and GRF data for each experimental trial to rigid body musculoskeletal simulation inverse kinematics analyses to estimate sagittal plane trunk, hip, knee, and ankle joint angles during stance phase of each trial.

Metrics representative of initial contact (IC) or the loading response (LR) phase of stance, as well as activity range of motion, were extracted to identify potential musculoskeletal adaptation strategies (Table 2.2).

Table 2.2: Joint kinematic metrics during stance phase

Joint/Segment	Sagittal
Trunk	Average Extension
Hip	1, 2, a
Knee	1, a
Ankle	3, a

1: Initial Contact ROM (peak flexion 0-25% stance - value at 0% stance); 2: Stance ROM (peak flexion - minimum flexion/maximum extension during stance); 3: Plantarflexion ROM (peak plantarflexion 0-25% stance - value at 0% stance)
a: Value at Initial Contact (0% stance)

Identification of "loading response" (0-25% stance) was selected as the portion of stance from heel strike at initial contact to the first loading peak of the vertical ground reaction force. While this differs from traditional definitions of phases of gait (Schmitz *et al.*, 2009), time ranges for the present study were selected to align adaptation strategies with the time points used in computational joint-level dynamic laxity simulations in Chapter 3 (Section 3.5). In particular, flexion angle at initial contact (0% stance) for hip, knee, and ankle were extracted, as well as range of motion (ROM) during loading response. Loading response ROM was defined as the difference between the peak value found in first 25% of stance and the value at initial contact. For ankle loading response ROM, plantarflexion-specific ROM was found as the difference between peak plantarflexion in the first 25% stance and ankle flexion at initial contact. If the foot was already in peak plantarflexion at heel strike, loading response ROM was set to zero (0°); no dorsiflexion ROM during this period of stance was calculated in order to have consistent sense of ROM during the loading response phase of stance. Additionally, hip flexion range of motion across stance phase of the gait trial and average trunk extension across stance phase were investigated. ROM

across the entire stance phase was calculated as the difference between maximum flexion and maximum extension (or minimum flexion). As an example, the metrics extracted for hip flexion are shown in Figure 2.4.

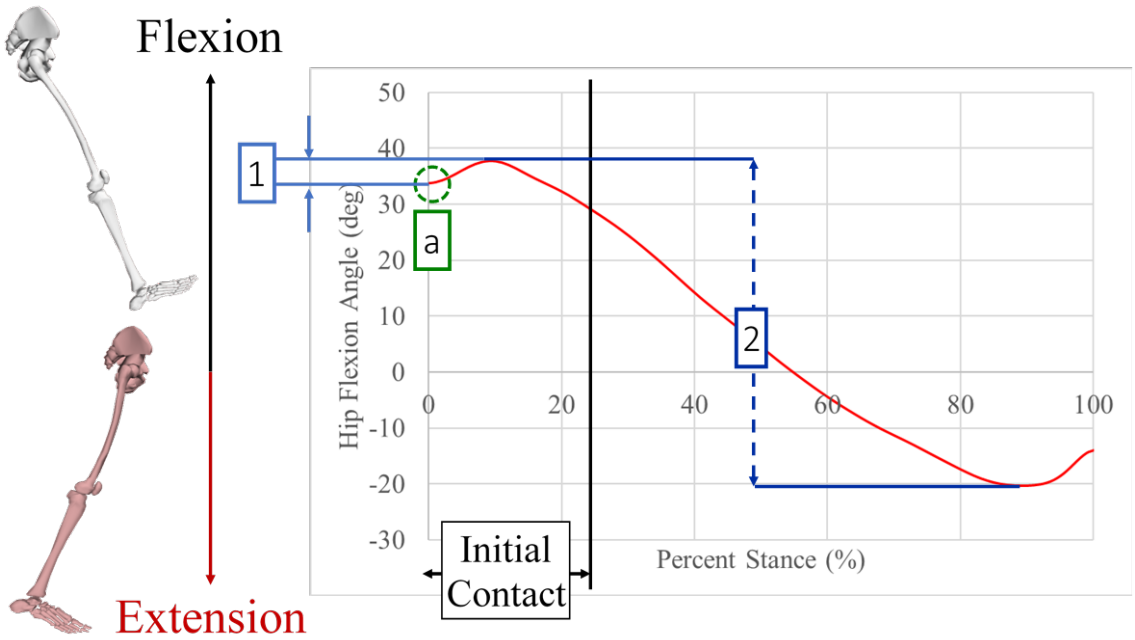

Figure 2.4: Hip sagittal plane kinematic metrics for a distracted walk activity on the uneven surface. 1: Initial Contact Range of Motion (ROM, peak flexion 0-25% stance - value at 0% stance), 2: Stance ROM (peak flexion - peak extension, 0-100% stance) and a: Value at Initial Contact (0% stance). Initial contact phase of stance is defined as the first 25% of stance (heel strike to first vertical loading peak).

Electromyography

Electromyography (EMG) signals were collected at 2400Hz using surface electrodes (Trigno, Delsys, Inc., Natick, MA) attached to the participant's dominant leg. Electrode were positioned on tibialis anterior (TA), gastrocnemius lateralis (GL), vastus lateralis (VL), rectus femoris (RF), vastus medialis (VM), medial hamstring (SM for semimembranosus), and lateral hamstring (BF for biceps femoris long and short

head) muscles according to Hermens et al. Before placing the electrodes, the participant's skin was shaved as necessary and cleaned with alcohol to reduce impedance (Hermens *et al.*, 2000). Proper placement of the electrodes were confirmed by viewing the EMG signals in Vicon while the participant activated the relevant muscles against manual resistance.

Collected EMG signals were processed using a Butterworth bandpass filter of 20-500Hz, full-wave rectification, and a Butterworth low pass, bidirectional second order filter with a cut-off frequency of 10Hz to create linear envelopes of the muscle activation signals (C-motion, 2020a). Signals were trimmed to stance phase and interpolated at 1001 points. The mean of the linear envelope of the EMG signal of the three trials for each condition were obtained and amplitude normalized to the peak muscle activity value for each muscle collected for a given participant.

Muscle activation strategies, assessed by percent co-contraction (% COCON) between agonist/antagonist muscles, was found for stance phase, as well as loading response (0-25% stance), mid-stance (25-75%), and terminal stance (75-100%) phases of gait. Division for these phases of interest came from timing of loading peaks for vertical GRF. Quadricep and hamstring % COCON was calculated using the equation proposed by Winter (2009) (Figure 2.5):

$$\%COCON = 2 * \frac{Common(A, B)}{Area(A) + Area(B)} * 100\%$$

where Area(A) is the area EMG activation profile for the sum of the quadriceps, Area(B) is the area for the sum of hamstrings, and Common(A,B) is the area under the EMG curve common to both muscle groups (Winter, 2009; Candotti *et al.*, 2009).

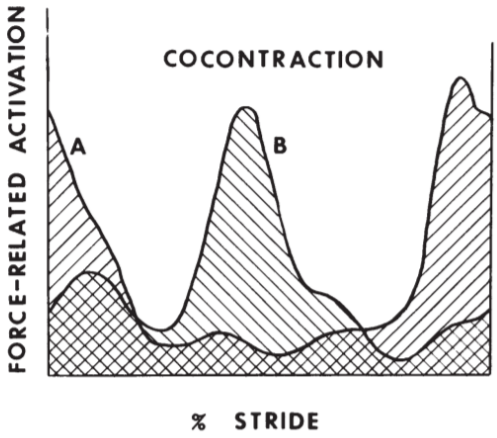

Figure 2.5: Agonist/antagonist muscle co-contraction. Cross-hatched area represents common area. (Adapted from Figure 6.9 in Winter, 2009).

Imbalances in quadricep and hamstring activation have the potential to increase risk for lower extremity injury. Quadriceps-dominant thigh muscle activation increases joint shear and anterior cruciate ligament loading. Co-activation of the hamstring muscles serves as a dynamic method of joint stabilization (Begalle *et al.*, 2012). Muscle synergy strategies and relative activation of quadricep versus hamstring muscles across stance phase were estimated via the quadricep-to-hamstring ratio (Q:H ratio) proposed by Begalle *et al.* by dividing the sum of the peak quadricep EMG activity (VM, RF, VL) by the sum of the peak hamstring EMG activity (SM, BF):

$$Q : H = \frac{\sum (max(VM), max(RF), max(VL))}{\sum (max(SM), max(BF)}$$

where Q:H = 1.0 indicates balanced co-activation for a given trial, Q:H $>$ 1.0 represents greater quadricep than hamstring activity, and Q:H $<$ 1.0 for hamstring muscle activity greater than quadricep (Begalle *et al.*, 2012).

Statistical Analysis

R statistical software (R Core Team, 2020) was used for all statistical analyses. Means and standard deviations were used to summarize participant characteristics. Age, sex, and surface conditions were considered independent variables while joint kinematics, peaks and impulse of ground reaction forces, and muscle co-contraction metrics were considered dependent variables. A three-way mixed analysis of variance (ANOVA) design was used to test the main effects and possible interactions between age, sex, and surface conditions. Significant main effects or interactions were submitted to Dunnett test multiple comparisons to determine differences from the baseline condition. Additionally, baseline metrics for young and older adults on the normal surface were compared using two-sample t-tests. An alpha level of $p<0.05$ was set *a priori* to denote statistical significance for all analyses.

2.3 Results

Kinematics

Significant differences were found for parameters for ankle, knee, hip, and trunk kinematics (Table 2.3).

Hip Flexion/Extension

An uneven surface reduced sagittal joint kinematics during the loading response segment of stance, indicating a surface-specific compensatory strategy. There was a surface main effect for hip flexion at initial contact. Participants stepped onto the uneven surface with hip joint more flexed, compared to the normal surface (30.9° vs

Table 2.3: Analysis of variance (ANOVA) results for kinematic parameters

Parameter	Age	Sex	Surface	Interaction	p-value
Ankle flexion - IC	0.848	0.733	**0.038***	age:surface	**0.014***
Ankle flexion - LR ROM	0.630	0.256	**<0.001***	age:sex	**0.023***
Knee flexion - IC	**0.012***	0.312	**<0.001***		
Knee flexion - LR ROM	0.114	0.313	0.688		
Hip flexion - IC	**0.030***	0.110	**<0.001***		
Hip flexion - LR ROM	0.337	**0.035***	**0.040***		
Hip flexion - Stance ROM	0.153	0.616	**<0.001***		
Trunk extension - Average	0.348	0.110	**0.015***		

Statistically significant age, sex, and surface main effects and any interaction effect p-values bolded and shown with * ($\alpha = 0.05$).
IC: initial contact (0% stance); LR ROM: loading response range of motion (heel strike to the first vertical loading peak at 25% of stance); Stance ROM: range of motion across stance phase of gait.

24.9°, $p < 0.05$). This increase in flexion at the hip at initial contact for the uneven surface resulted in, seen by a surface main effect, an increased joint range of motion (the difference between peak flexion and peak extension) across stance phase (42.4°), compared to both normal (36.0°, $p < 0.001$) and slick (37.5°, $p < 0.001$) surfaces (Figure 2.6).

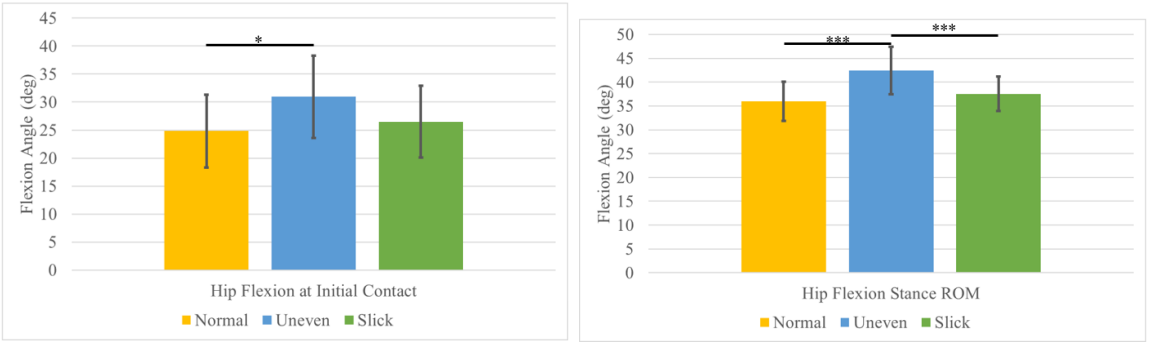

Figure 2.6: Surface main effect for hip flexion at initial contact (left) and range of motion across stance (right) [*p<0.05, ***p<0.001].

There was a significant sex main effect for hip flexion during loading response with female participants exhibiting a greater range of motion, compared to males (12.1° vs 9.5°, $p < 0.001$) despite flexion angles at initial contact that were not significantly different between sexes (Figure 2.7).

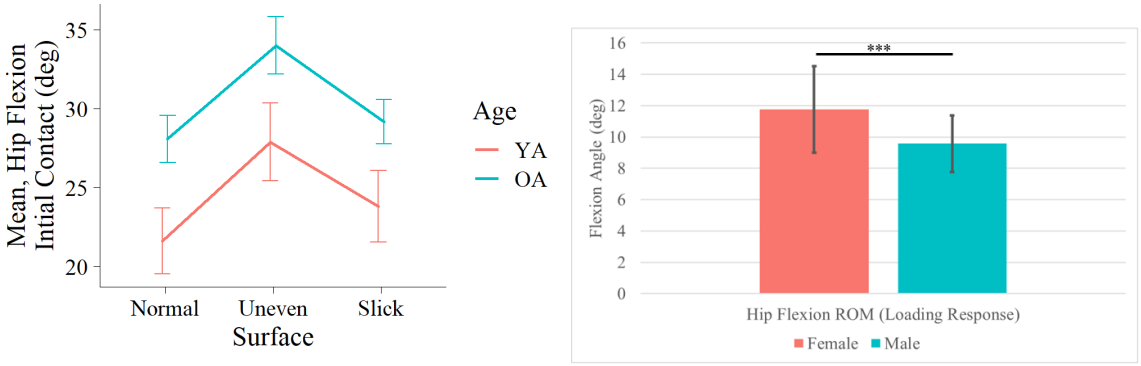

Figure 2.7: Hip flexion at initial contact (left). Sex main effect for hip flexion range of motion during stance (right). YA: young adults and OA: older adults [*p<0.001].**

There was a significant age affect for hip flexion at initial contact where older adults adopted a hip flexion strategy comparable to that seen when looking at the uneven surface, approaching all surfaces with greater hip flexion (30.4°) than younger adults (24.4°, $p < 0.001$; Figure 2.8). Assessing and comparing baseline metrics for young and older adults on the normal surface, older adults had significantly higher hip flexion at initial contact (28.1°), compared to young adults (21.6°, $p<0.01$).

Knee Flexion/Extension

This tendency of older adults to prepare for and step onto the uneven surfaces in a more conservative manner was also seen in an age main effect for knee flexion at initial contact, compared to young adults (14.5° vs 7.2°, $p < 0.001$). The surface-

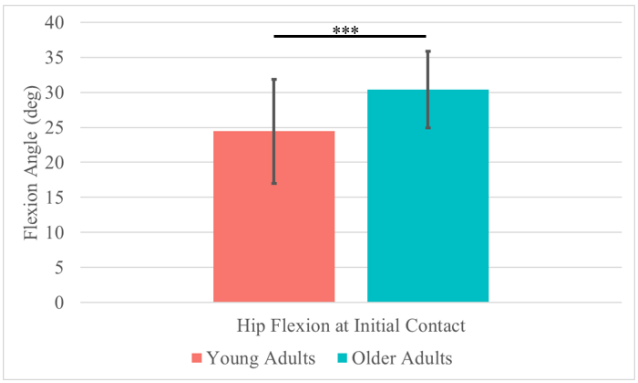

Figure 2.8: Age main effect for hip flexion at initial contact [*p<0.001].**

specific adaptation observed with hip flexion continues down the kinematic chain to the knee with a surface main effect where gait on an uneven surface increased knee flexion at initial contact, compared to both normal (15.8° vs 7.5°, $p < 0.01$) and slick (15.8° vs 9.2°, $p < 0.05$) surfaces (Figure 2.9). Knee flexion at initial contact on the normal surface was higher for older adults (10.8°) than the young adult baseline (4.1°, $p<0.05$).

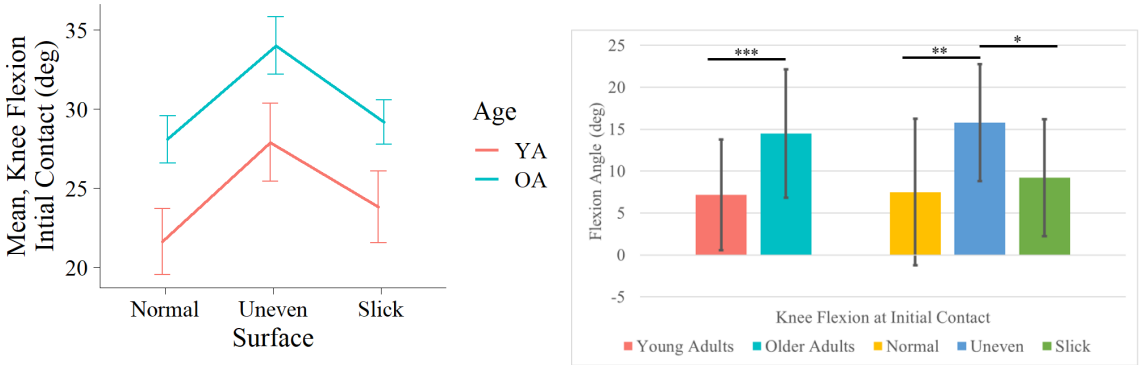

Figure 2.9: Knee flexion at initial contact. YA: young adults and OA: older adults [*p<0.05, **p<0.01, ***p<0.001].

Ankle Plantarflexion

For plantarflexion at initial contact, there was a significant age*surface interaction

where older adults stepped onto the uneven surface with the dominant foot in a more neutral position (slightly plantarflexed) compared to the normal surface (-0.8° vs 3.9°, $p < 0.05$). No significant surface effect was observed for younger adults where all younger participants landed, regardless of surfaces, in a more neutral pose with foot in slight dorsiflexion (Figure 2.10). A more negative value for ankle flexion indicates more plantarflexion while a flexion angle closer to zero indicates a neutral foot position.

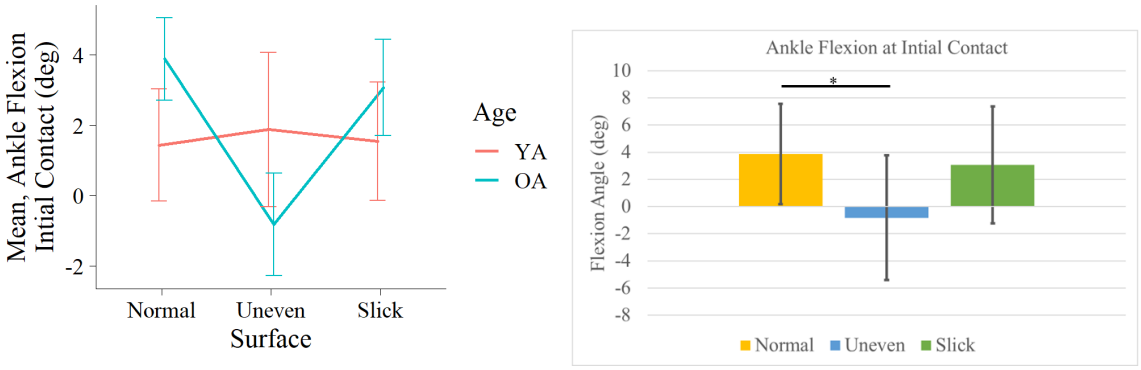

Figure 2.10: Ankle flexion at initial contact (IC, left). Surface effect for older adult ankle plantarflexion at IC (right). YA: young adults and OA: older adults [*p<0.05].

However, regardless of age, the uneven surface resulted in decreased plantarflexion range of motion during the initial loading response (surface main effect), compared to the normal surface (-2.3° vs -7.0°, $p < 0.001$). There was also a significant age*sex interaction effect where older adult females were more conservative in their ankle range of motion, regardless of surface resulting in -3.8° range of plantarflexion motion, compared to nearly twice that (-6.6°, $p<0.05$) for their older male counterparts (Figure 2.11).

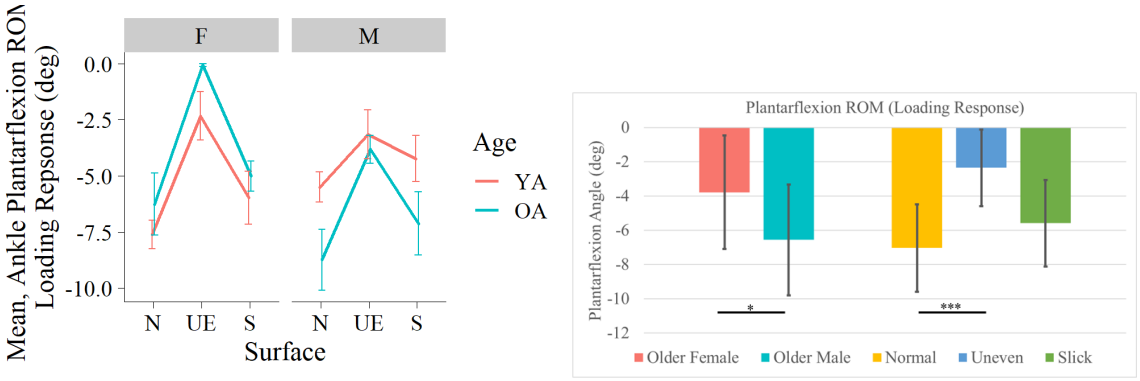

Figure 2.11: Ankle plantarflexion range of motion (ROM) during loading response (left). Surface- and age-specific sex (right) differences for ankle plantarflexion ROM during loading response. YA: young adults, OA: older adults; F: female, and M: male; N: Normal, UE: Uneven, S: Slick [*p<0.05, ***p<0.001].

The age and surface related changes to flexion angles at initial contact can be visualized across the kinematic chain connecting trunk, hip, knee, and ankle (Figure 2.12). Similar angles were seen for older adults as on the uneven surface. While there was a significant surface main effect for average trunk extension across stance, pairwise comparisons were not significant. However, participants did tend to respond differently to the different challenging surfaces by leaning further forward on the uneven surface, compared to the slick surface (-9.2° versus -7.2°, p=0.672).

Ground Reaction Force

Significant differences were found for anteroposterior impulse and vertical ground reaction force parameters (Table 2.4).

This anticipatory or cautious musculoskeletal adaptation of older adults was also seen in a significant age main effect for the vertical component of the ground reaction

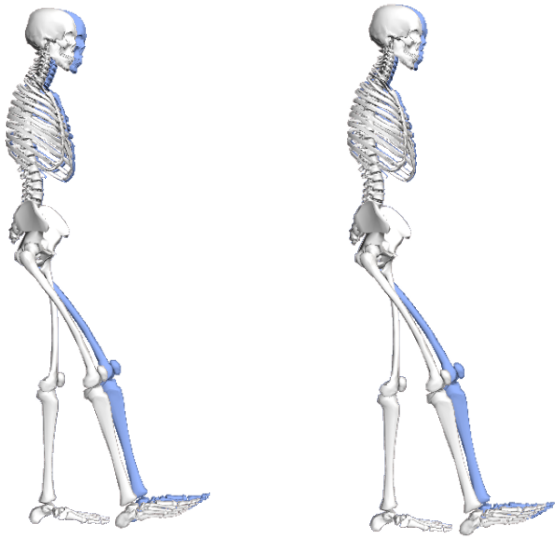

Figure 2.12: Kinematic chain at initial contact for young versus older (blue) adults (left) and normal versus uneven (blue) surfaces (right).

Table 2.4: Analysis of variance (ANOVA) results for kinetic parameters

Parameter	Age	Sex	Surface	Interaction	p-value
Breaking Impulse	0.445	0.113	**0.015***		
Propulsive Impulse	0.427	0.874	**0.019***		
1st Loading Peak	**0.039***	0.536	0.378		
Loading Rate	0.214	0.701	0.638		
2nd Loading Rate	0.540	**0.016***	0.100	age:surface	**0.030***

Statistically significant age, sex, and surface main effects and any interaction effect p-values bolded and shown with * ($\alpha = 0.05$).

force. Older adults were overall more cautious than younger adults with a lower peak magnitude of initial vertical ground reaction force (OA: 100.1% BW vs YA: 104.3% BW, $p < 0.001$). No statistically significant age-related differences were found for the vertical component of the ground reaction force for the remainder of stance phase. However, there was found a significant sex main effect for the magnitude of the second loading peak. Females used 96.4% of their body weight at this second peak, compared to males who used 100.8% BW ($p < 0.001$). There was no significant sex difference in the initial loading peak (Figure 2.13). While a significant age*surface interaction was found for this second peak, pairwise comparisons were not found to be significant. For the baseline condition on the normal surface, young adults had higher initial loading peak force (105.64% BW) than the older adults (99.98% BW, $p<0.05$).

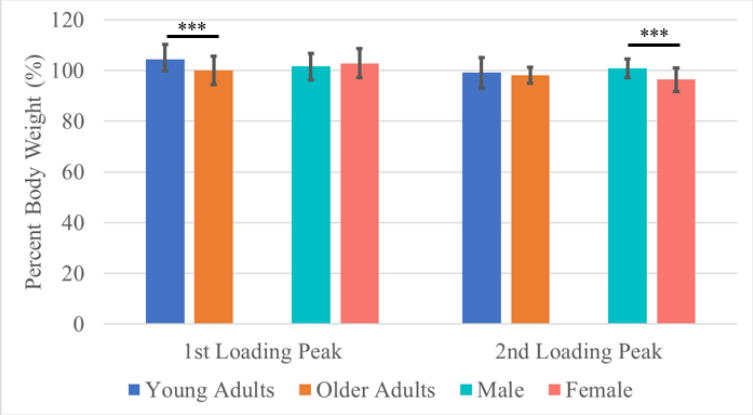

Figure 2.13: Vertical ground reaction force for initial loading response (age main effect) and second loading peak (sex main effect) [*p<0.001].**

While significant surface effects were found for both breaking and propulsive impulses, no significant pairwise comparisons were observed for the x-component of the ground reaction force. However, the slick surface tended to reduce the ability of participants to slow their center of mass during the initial loading phase of stance as

seen in reduction in magnitude of breaking impulse on slick surfaces compared to the normal surface (-4.5 N $\frac{\%stance}{\%BW}$ vs -5.3 N $\frac{\%stance}{\%BW}$, p=0.0943). A larger negative value indicates a greater magnitude of breaking impulse. Additionally, the uneven surface tended towards increasing propulsion in the later part of stance as seen in increased propulsive impulse on uneven surfaces, compared to the normal surface (2.4 N $\frac{\%stance}{\%BW}$ vs 1.9 N $\frac{\%stance}{\%BW}$, p=0.0588).

Muscle Activation

Significant differences were found for quadricep-hamstring co-contraction during terminal stance (Table 2.5).

Table 2.5: Analysis of variance (ANOVA) results for quadricep-hamstring co-contraction

Parameter	Age	Sex	Surface	Interaction	p-value
Loading Response	0.251	0.712	0.311		
Mid Stance	0.933	0.647	0.052		
Terminal Stance	0.991	0.207	0.829	age:sex:surface	**0.042***
Full Stance	0.697	0.447	0.067		
Q:H Ratio	0.991	0.318	0.368		

Statistically significant age, sex, and surface main effects and any interaction effect p-values bolded and shown with * ($\alpha = 0.05$).
Loading response is 0-25% stance phase, mid stance is 25-75% stance, terminal stance is 75-100% stance, and full stance co-contraction is for quadricep-hamstring co-contraction across 0-100% stance. Q:H ratio is a measure of quadricep to hamstring relative activation and synergy.

During the preparation or terminal stance phase of stance, there was a significant three-way interaction (age*sex*surface) effect for the percent co-contraction between the quadricep and hamstring muscles with significant sex differences, for older adults on the slick surface (Figure 2.14). These muscle groups were activated simultaneously

82.8% of the terminal stance phase for older females, but only 61.9% for older males when walking on the slick surface ($p < 0.001$). Overall, males tended to require lower levels of co-contraction during terminal stance than females (67.7% versus 74.4%), though this difference was not found to be significant.

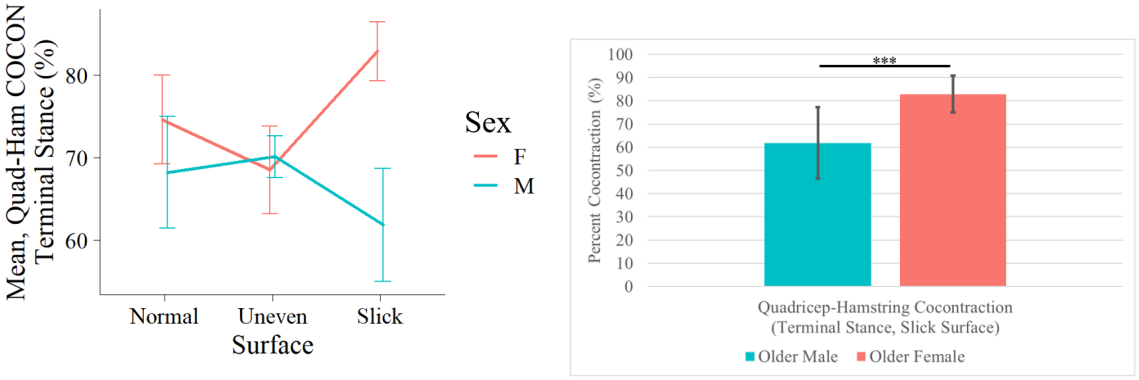

Figure 2.14: Sex differences for percent co-contraction of quadriceps and hamstrings for older participants on the slick surface during terminal stance. F: female, and M: male [*p<0.001].**

No statistically significant differences were found for the quadricep-to-hamstring ratio for walking on different surfaces. Both age groups demonstrated comparable synergy activation strategies across stance while challenging surfaces reduced the Q:H ratio, resulting in more balanced quadricep and hamstring activation (Table 2.6).

Table 2.6: Quadricep:Hamstring (Q:H) ratio across ages and surfaces

Group	Q:H	Main Effect (p-value)
Young Adults	1.607	0.991
Older Adults	1.605	
Normal	1.744	0.368
Uneven	1.614	
Slick	1.458	

2.4 Discussion

The objectives of this study were to compare joint kinematics, ground reaction force loading patterns, and muscle activation strategies for young and older adults walking across various challenging surfaces to identify potential adaptation strategies and to assess how these adaptations change with age.

The findings of this study show that an uneven surface results in a more flexed leg during stance, regardless of age. Additionally, older adults adopt a more conservative pose, seen as increased flexion angles resulting in more bent limbs, when walking, regardless of surface. Vertical loading patterns changed with age during the initial loading response portion of stance phase but no significant age differences in adaptations were seen for the remainder of stance. Surface design and selection of gait as activity of interest in this analysis did not reveal any surface- or age- specific adaptations to challenging conditions for breaking or propulsive impulses and muscle co-contraction during early portions of stance.

Surface-related changes to challenging surfaces

Challenging surfaces, specifically the uneven surface, increased sagittal plane angles for hip, knee, and ankle, in agreement with our second hypothesis. Plantarflexion range of motion during the initial loading response decreased on the uneven surface, likely caused by the surface-driven changes in foot placement at initial contact. The decreased dorsiflexion for the uneven surface is agrees with Dixon *et al.*. Differences in ankle flexion at initial contact impact flexion for the other joints up the kinematic chain. Specifically, the uneven surface increased knee and hip flexion at initial contact, in agreement with prior research (Dixon *et al.*, 2018; Saywell *et al.*, 2012; Hinman

et al., 2002). This adaptation might improve stability on the challenging surface by lowering the center of mass.

While not found to be significant, participants did tend to lean further forward when walking on the uneven surface, perhaps looking down at their feet more. However, due to the marker set used and lack of data regarding eye motion, it cannot be verified if participants adapted to walking on an uneven surface by changing their gaze. While also not found to be statistically significant, the slick surface tended to reduce the ability of participants to slow their forward momentum when encountering the slick surface, potentially reducing stability. Surface main effects were found for both propulsive and breaking impulse; however, the pairwise comparisons were not significant suggestive of more participants needed in order to clarify these findings.

Age-related changes

Older adults tended to adopt a more conservative pose throughout the walking trials, regardless of surface. This pose is similar to that of the uneven surface with increased hip and knee flexion, compared to younger adults. Additionally, the older adults were more cautious early in stance, as seen by decreased vertical loading. No differences had been observed in vertical loading for older adults during stair descent by Saywell *et al.* (2012). This may be an activity related difference in loading patterns. In later stance, age-related adaptation transitions to sex differences as females are more cautious in the second loading peak and older females use increased quadricep and hamstring co-activation on slick surfaces during the preparation phase of terminal stance. Saywell *et al.* (2012) found age-related decreases in the ability to attenuate impulse, specifically during stair descent. These differences were not

observed here, perhaps due in part to looking at gait versus stair descent, which is a more demanding activity. All Q:H ratio values for this study, 1.46 for slick gait - 1.74 for gait on the normal surface, were less than those found by Begalle *et al.* (2012) for more physically demanding closed kinetic chain exercises: 2.87 for single-limb dead lift - 9.70 for forward lunge (Begalle *et al.*, 2012). Expansion of this analysis to other activities is necessary to investigate potential activity related differences and activity-specific adaptation strategies. For all neuromechanics metrics other than knee and hip flexion at initial contact and initial vertical loading peak, young and older adults had similar baseline metrics, which is in good but not full agreement with our first hypothesis.

Study Limitations

There were a few limitations in the study design of this experiment. The uneven surface used for this experiment is contrived without many common analogs that people would encounter during activities of daily life. Therefore, the adaptations to this uneven surface may not be completely transferable to surfaces with lower variations in height such as cobblestone, natural surface trails, or the experimental walkway used by Dixon *et al.* (2018). However, while this uneven surface, like those manufactured from blocks placed under a malleable surface (Thies *et al.*, 2005), may not completely represent real-world surfaces, Dixon *et al.* (2018) suggested that larger changes in surfaces would result in larger changes in gait such that the results found here would likely be representative of the direction of changes and adaptations occurring for less abrupt uneven surfaces, if perhaps larger in magnitude here (Dixon *et al.*, 2018).

The cohorts of interest for this study were selected to be healthy young adults

and older adults with a history falling. While this selection does not include healthy older adults, potentially obscuring which differences and adaptation strategies stem from strict age differences versus differences related to having previously fallen, the goal with this choice of cohorts was to identify the biggest difference between young healthy adults and older adults who are vulnerable to falling.

2.5 Conclusion

Overall, uneven surfaces result in conservative kinematics to maintain stability during gait. Further analysis will investigate different surfaces and conditions across other activities to expand upon musculoskeletal adaptation to external challenging conditions and how this adaptation changes with age.

Insight into joint stiffening and other adaptation strategies resulting from this research will be used to inform future analysis investigating joint-level adaptations as well as assessment of joint stiffness, stability, and laxity. Understanding the relationships between joint-level stability and whole-body musculoskeletal function has the potential to inform targeted muscle training programs and joint-level interventions to improve whole-body musculoskeletal function and reduce risk of human injuries. Additionally, the results of this study may facilitate future research into the ability of the musculoskeletal system to adapt to changing surroundings and how this ability changes with age.

CHAPTER 3:
FINITE ELEMENT MODEL DEVELOPMENT AND DYNAMIC LAXITY

3.1 Introduction

Knee joint stability is a known risk factor contributing to accidental falls. Knee instability, as identified as knee buckling or giving way or slippage of the knee without buckling, results in a 4.5-fold increase in risk of recurrent falls (Nevitt *et al.*, 2016; Schrager *et al.*, 2008). Joint stability also influences joint loading, cartilage wear, and mobility for maintaining independence in the older adult population. Muscle co-contraction around the knee improves tibiofemoral stability, protecting the cruciate ligaments from damage (Li *et al.*, 1999; Hallal *et al.*, 2013). However, excessive co-contraction increases metabolic cost leading to fatigue and increased risk of falling. Additionally, increased co-contraction can result in excessive loading and wear of the cartilage, contributing to the development and progression of osteoarthritis. This compensatory strategy may not be effective as a dynamic strategy to circumvent a fall immediately after tripping (Hallal *et al.*, 2013). Given the links established in prior research between knee stability and risk of falls, evaluation of knee joint stability, and correlation with whole-body neuromechanics, may provide additional insight into the risk of falling in older adults.

Direct *in vivo* measurement of soft-tissue loads and ligament engagement is not practical for ethical and logistical reasons. Current knee laxity and *in vivo* evaluation of knee joint stability is accomplished via basic clinical tests such as the anterior drawer and Lachman tests. These passive tests do not consider the compressive loading across the joint resulting from muscle activation and ground reaction force. Some cadaveric or computational studies apply a compressive load across the joint and measure displacements and rotations resulting from applied external loads (Harris *et al.*, 2016; Athwal *et al.*, 2019). Specifically, researchers using the Oxford knee rig applied 710N axial load to simulate weight-bearing while applying $\pm$150 N anterior-posterior loads at flexion angles ranging from full extension to 90° (Athwal *et al.*, 2019). While these studies are an improvement upon the clinical passive laxity tests, they still neglect the *in vivo* response of increased muscle co-activation to avoid or reduce excessive motion during activities of daily life. Therefore, there exists a need for a new quantitative method for evaluating dynamic knee joint stability under physiological muscle loads.

In order to investigate the underlying mechanisms of musculoskeletal adaptation and establish relationships between whole-body adaptation and joint-level stability, experimental and musculoskeletal modeling was combined with subject-specific finite element models. In this thesis work, a proof-of-concept knee joint stability assessment and model development pipeline was developed and implemented using subject-specific models from one older and one younger participant during stance phase of gait. Quadricep, hamstring, and shank muscle forces, in addition to ground reaction forces, were applied to subject-specific finite element models. Subsequent external loads were applied to the tibia. Resulting anterior-posterior displacements and varus-

valgus and internal-external rotations during each test were used as a novel metric of functional stability. In future work, this stability assessment will be applied to the larger dataset to investigate the relationship between knee joint laxity/stability and age-related whole-body motions and muscle co-activation strategies.

3.2 Clinical Coordinate System Definition

Dominant limb lower extremity kinematics were calculated from participant motion capture trials for use in the finite element model framework. There are inherent limitations of motion capture. For example, during experimental motion capture data collection, markers placed on or over soft tissue, such as the thigh and greater trochanter, result in greater movement artifact and reduced accuracy for non-sagittal plane kinematics (Cappozzo *et al.*, 1996). Additionally, rigid-body musculoskeletal models, such as OpenSim, do not incorporate tibiofemoral soft tissues such as cartilage and ligaments. Consequently, axial and coronal kinematics that can be calculated via inverse kinematics analyses in OpenSim from experimental marker locations are not as trustworthy as the resulting tibiofemoral motion driven by geometry in the finite element model. Additionally, there exists differences in definition of clinical kinematic axes between OpenSim and the finite element model. To ensure accurate and consistent kinematic axes between marker trajectories and MRI geometry, model state coordinates from static optimization were used to calculate joint kinematics, using the method presented by Grood and Suntay 1983.

A joint coordinate system was defined for each of the hip, knee (tibiofemoral, TF), and ankle joints according to Grood and Suntay such that the axes have clinical sense and are based on the local coordinate system defined on each bone (Grood & Suntay, 1983). The hip joint is defined by the mediolateral (ML) axis of the

pelvis, the superoinferior (SI) axis of the femur, and the floating anteroposterior (AP) axis as the cross product of the ML and SI axes such that the joint AP axis is orthogonal to both the ML and SI axes. The TF joint is defined by the ML axis of the femur and the SI axis of the tibia. The ankle joint is defined by the ML axis of the talus and the SI axis of the tibia. The clinical ML, AP, SI axes on each bone were defined using bony geometry, where possible, augmented with experimental marker coordinates. For example, the ML axis of the femur is defined as passing through the medial and lateral epicondyles and the SI axis of the femur passes through the knee joint center, as defined by the mid-point of the epicondyles, and the hip joint center calculated from experimental markers as outlined in Section 2.2 for the functional hip trials. A transformation matrix was based on the relative pose between the local coordinate systems of both bones in the specific joint of interest. Joint kinematics, both translations along and rotations about these joint axes, were calculated using the equations proposed by Grood and Suntay with the use of atan2 instead of atan (Grood & Suntay, 1983; Milholland, 2019) to check proper quadrant predicted for flexion-extension angle, mainly at the hip and ankle.

The kinematic pose for the static trial used in aligning OpenSim and MR geometry as will be outlined in Section 3.3 as well as all frames of a given motion trial can be derived using the coordinates of the nodes used in the definition of the axes and the equations proposed by Grood and Suntay. In order to apply these static kinematics to connector elements in the finite element model, correction factors were needed to account for effective translation along the SI and ML axes due to rotation about the AP axis (Milholland, 2019).

3.3 Subject-specific 3D Knee Model Development

A detailed 3D model of each experimental participant was developed for the dominant knee composed of rigid bones, articular cartilage, non-linear tension-only spring-based ligaments, elastic tendons, and quadriceps muscle representations. Subject-specific geometry was derived from supine 3T magnetic resonance (MR) imaging of the dominant knee with 1mm slice thickness and 0.2188mm in-plane resolution. Commercial software (Amira, FEI, Hillsboro, OR) was used to extract from the MR images contours for bones, cartilage, menisci, and the quadricep tendons. Supplementing the extracted contours, the attachment location and gross dimensions and orientations were obtained for the rectus femoris (RF), vastus lateralis (VL), vastus intermedius (VI), vastus medialis (VM), and patellar ligament (PL). These values were used in a custom Python algorithm to convert the tendons to equivalent 2D fiber-reinforced membranes with attachment sites for the respective quadricep muscles. Cartilage and meniscal structures were re-meshed after Amira segmentation to create regular hexahedral elements using custom MATLAB scripts from a publicly available software repository housed at the University of Connecticut (Rodriguez-Vila *et al.*, 2017). The automated hexahedral meshing code was supplemented in-house to mesh the patellar cartilage and blend patellar and femoral cartilage into the respective bones to decrease edge loading in subsequent computational analyses. The process for generating subject-specific geometry from MR imaging can be visualized in Figure 3.1.

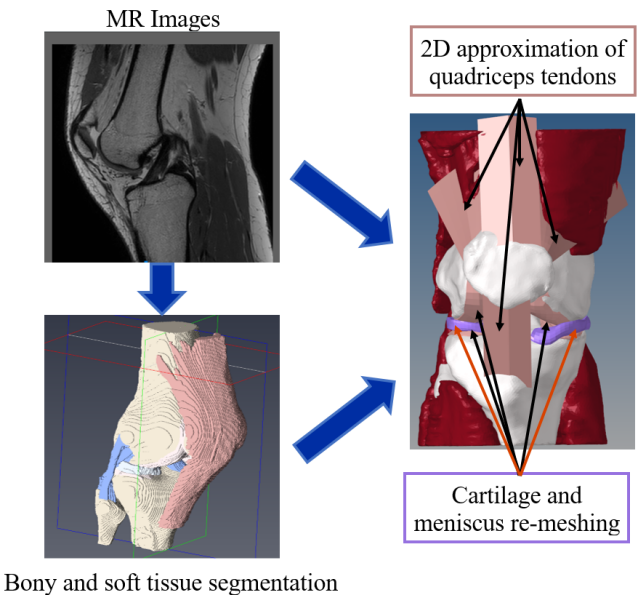

Figure 3.1: The pipeline to create subject-specific geometry from participant MR imaging of the knee.

3.4 Lower Limb Finite Element Model

The rigid-body musculoskeletal and subject-specific 3D models described in Sections 2.2 and 3.3 were combined to create a lower limb finite element model in Abaqus/Explicit (Simulia, RI). There exist different coordinate systems and orientations from the OpenSim and MR geometry, as well as between the starting pose for the static and experimental trials. Bony geometry coordinate systems were aligned using an iterative closest points algorithm, with resulting transformations applied to align all geometry into a uniform simulation starting pose for each subject-specific finite element model.

Generic OpenSim bone geometries, scaled using the same scale factors used in Section 2.2 derived for a given participant, were transformed from coordinates systems local on each bone to an assembled global coordinate space, relative to a global origin

located at the knee joint center, as defined by the midpoint between the femoral epicondyles. Next, the MR geometry was aligned to the global coordinate system. The placement of the participant's leg in the MRI machine is slightly flexed; therefore, the global OpenSim geometries are subsequently aligned to this flexed limb alignment. Following alignment of subject-specific geometry, generic representations for muscles and tibiofemoral ligaments were scaled and aligned to the final global scan space.

Specifically, to accomplish the alignment of OpenSim and MR geometry, anatomic mediolateral, anteroposterior, and superoinferior axes were defined for the OpenSim bones using the location of experimental markers in the first frame of the static trial. Transformation matrices resulting from these axes were used to convert from local OpenSim to global simulation coordinate systems. Next, the MR geometry was aligned to the global coordinate system via an iterative closest points (ICP) algorithm, using kDtree for point matching. kDtree is a MATLAB function from the Statistics Toolbox performing a k-nearest-neighbor search using a kd (k-dimensional) tree to minimize distance between three-dimensional point clouds. The resulting rotation and translation matrices from the ICP alignment procedure were used to move all MR geometry to the global simulation space. A second round of ICP alignment was used to align the lower leg and foot OpenSim geometries to the flexed scan space of the MR geometry (Figure 3.2).

Physiological lines of actions for the musculature of the lower limb were obtained from the publicly available Visible Human Project datasets. The centroid for each muscle modelled in the OpenSim generic model was obtained from the three-dimensional Visible Human geometry for the respective muscle. Subject-specific lines of action for these muscles were created by mapping the generic lines of action to

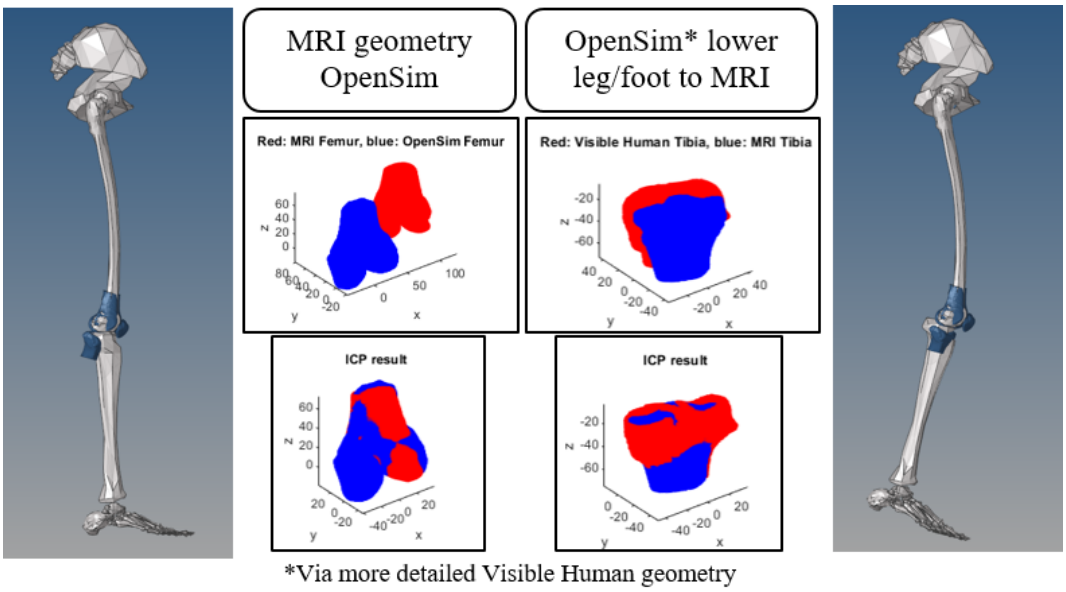

Figure 3.2: Iterative Closest Points (ICP) procedure for aligning geometry to a common, global scan space. Left: OpenSim geometry (white) and MRI geometry (blue) in global space. Right: OpenSim tibia and foot geometry aligned to MRI scan space.

the length and attachment sites of the muscles in OpenSim. The attachment site for the quadriceps muscles were derived from the 2D fiber-reinforced membranes generated for the respective quadricep tendons. These muscle geometries were aligned to the global scan space coordinate system from a local OpenSim starting point in the same manner as above, with muscles with attachment sites on the tibia and below undergoing both sets of ICP alignment regimens.

The final step in the development of the subject-specific lower limb finite element model was the alignment of scaled generic tibiofemoral ligament geometries to the final global MRI scan space. The coordinates for femoral and tibial ligament attachment sites were derived from the publicly available DU01 online dataset (Harris *et al.*, 2016). Further detail regarding specific ligaments modeled and finite element representation

can be found in Table 3.1. Materials properties were based on experimental values used in previously validated models (Blankevoort & Huiskes, 1991, 1996; Pandy *et al.*, 1997; Harris *et al.*, 2016).The DU01 femur and tibia, scaled in the mediolateral and anteroposterior directions to align with subject-specific bony geometry, were aligned separately to the MR femur and tibia, respectively, in global space using the same iterative closest points procedure. The resulting rotation and translation matrices were applied to the relevant femoral or tibial attachment coordinates of each ligament. The resting length of each ligament was derived from the final attachment coordinates.

3.5 Dynamic Laxity Methods

The lower-extremity finite element model development pipeline outlined above was employed to created aligned subject-specific geometry for a male younger (22yr, 175.3 cm, 71.2 kg) and a female older participant (67yr, 155.0 cm, 47.2 kg) from the cohort collected in the Center for Orthopaedic Biomechanics Research lab. These participants were intentionally selected for the difference in age, gender, and size to demonstrate that this analysis can be applied to a broad population cohort. Estimates for muscle forces and related joint angles were extracted using static optimization in OpenSim for four "snapshot" poses during stance phase of a walking trial on the slick surface. The following definitions were used for the four snapshot poses across stance: heel strike (HS, 0% stance), first vertical loading peak (F1, 25%), second vertical loading peak (F3, 75%), and toe off (TO, 100%).

The maximum isometric force for each muscle in the generic OpenSim model was scaled for each participant using collected subject-specific maximum isometric strength measured by a Humac Norm dynamometer (Tables B.1 - B.2). The flexion/extension activities performed using the dynamometer were emulated in Open-

Table 3.1: Tibiofemoral ligament properties

Ligament	Bundles	Elements	Linear Stiffness [N/ϵ]	Reference Strain[a]
Anterior Cruciate Ligament (ACL)				
Posterolateral	1	2	2694	1.01
Anteromedial	1	2	3239	1.02
Anterolateral Ligament (ALL)	1	3	1339	1.18
Lateral Collateral Ligament (LCL)	1	3	5551	0.98
Medial Collateral Ligament (MCL)				
Deep	1	3	4008	1.02
Superficial (anterior, mid, posterior)	1	3	3463, 3587, 3412	0.97, 1.04, 1.00
Posterior Cruciate Ligament (PCL)				
Anterolateral	1	2	4252	0.85
Posteromedial	1	2	4312	0.95
Posterior Oblique Ligament (POL)	1	2	1290	1.12
Posterior Capsule (PCAP)				
Medial	1	3	2830	1.01
Lateral	1	3	2591	1.03
Popliteal Fibular Ligament (PFL)	1	3	1585	1.04

[a] At full extension, if reference strain (EREF) = 1.0, the ligament is at the slack length; EREF $>$ 1.0: ligament is slack; EREF $<$ 1.0: ligament is taut.

Material properties presented are an average of those found by Blankevoort & Huiskes, 1991, 1996; Pandy *et al.*, 1997; Harris *et al.*, 2016.

Sim by positioning the scaled model in the experimental poses and running forward dynamics simulations to estimate joint moments. Resulting moments were compared to the recorded experimental torques, scaling muscle forces required to match these moments. These scaling factors were used to scale the maximum isometric force of the OpenSim muscles used in the model for static optimization analyses. Static optimization was used to estimate individual muscle forces required to produce the joint motions observed experimentally, solving equations of motion while minimizing the sum of the squared muscle activations at each time step.

Muscle forces and joint coordinates (transformed to global OpenSim space) were extracted from the static optimization results for the four snapshot poses. Hip, knee, and ankle kinematics for each snapshot pose were calculated according to the method presented in Section 3.2 (Figure 3.3).

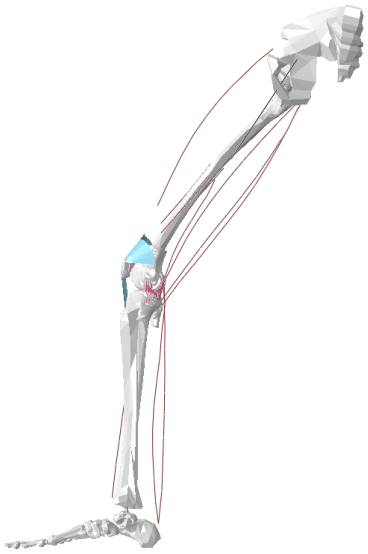

Figure 3.3: Younger adult OpenSim and MR geometry, with muscle and ligament representations, aligned into global scan space and subsequently moved to starting pose for heel strike snapshot.

Since the knee geometry derived from the MR images were in an unloaded supine position, but the assembled and aligned finite element model is vertical, the position of the patella was unconstrained kinematically and allowed to settle into position via applied forces and contact mechanics. The quadriceps muscles applied force to the patella via their respective tendons. A minimum threshold muscle force was set at 15N for small OpenSim muscle excitation predictions to maintain force in all the muscle elements and keep quadriceps tendons taut and maintain contact of the patella with the knee joint. The mediolateral, vertical, and anteroposterior components of the experimental ground reaction force were applied to the reference node for the OpenSim talus bone to provide joint compressive force.

The aligned participant geometry from Section 3.4 was moved from the starting MRI pose in global scan space to the pose dictated by calculated joint kinematics while muscle forces were ramped to activations predicted by OpenSim for that same pose. Apart from maintaining tibiofemoral flexion throughout the simulation, all other degrees of freedom at the knee joint were free, allowing the geometry to settle into a neutral position. This method corrects for potential differences between the supine MRI and vertical snapshot poses. In this snapshot pose, hip and ankle kinematics, knee flexion, ground reaction force, and muscle forces were held constant. Loads and torques intended to assess the stability and laxity of the knee joint were applied and resulting motion of the knee were calculated for comparing across stance phase as well as between older and young adult participant simulations. Applied loads were as follows:

- Anterior/posterior: ± 1500 N
- External/internal: ± 25 N m
- Valgus/varus: +25 N m / −15 N m

For all trials, SI translations were controlled by the applied ground reaction force. For AP tests, IE rotation and ML translation were held constant. IE rotation and AP and ML translations were held constant for VV trials. AP and ML translations were held constant for IE trials. The external loads applied here exceed that of those employed by Harris *et al.* (2016) and Ball *et al.* (2020) in their experimental and computational assessment of knee joint laxity. Their experiments applied ± 80 (90) N AP force, ± 8 (5) Nm IE torque, or ± 10 (8) Nm VV torque, values in parentheses are from Ball *et al.* 2020. Harris *et al.* (2016) also applied a 20N compressive load to maintain tibiofemoral contact during testing. However, with the inclusion of physiological muscle and ground reaction forces, the compressive load across the TF joint was significantly larger in the present simulations and therefore greater external loads need to be applied in order to generate displacement and rotation movements that are clinically meaningful. Disparate magnitudes of valgus and varus torque were applied because larger varus torques resulted in model instability and joint dislocations.

Resulting relevant displacements and rotations from applied external loads (i.e. anterior displacement for applied anterior load) were compared for each participant across the snapshot phases of stance. Net joint compressive loads at each of the snapshots were also compared. Combining trends in both joint motions and compressive joint loading, potential trends in co-activation and joint stiffening mechanisms were investigated.

3.6 Results

Resulting joint motions for each snapshot pose, laxity test, and knee are presented in Table 3.2.

During the initial loading response, at the first loading peak of the ground reaction force, the older knee had a greater compressive load applied across the joint, as measured by the sum of the quadriceps, hamstrings, and gastrocnemius muscles and the magnitude of the ground reaction force. However, for all other snapshots of stance phase, the younger knee had a greater compressive force, expressed in terms of percent body weight.

All laxity motions for the older adult were less than that of the younger adult, except for posterior displacement at the second loading peak and varus rotation at heel strike and toe off (Figure 3.4).

3.7 Discussion

The preliminary results presented here represent proof-of-concept for the development of subject-specific dynamic laxity tests that apply physiological muscle and ground reaction loads. Further analysis is required to determine if the trends identified between these participants will hold when expanding the analysis to include all experimental participants.

Decreased displacement and rotation under corresponding applied load and torques is suggestive of adaptation strategies to reduce joint motion and improve stability. However, since the sum compressive load applied is only greater for the older adult during the first loading peak, there may be other strategies employed for joint stiffening. Combining the results of Chapter 2 with these current dynamic laxity findings,

Table 3.2: Displacements and rotations resulting from applied laxity loads and torques for each snapshot pose during stance

Pose	Loading DOF	Knee	Resulting Motion
HS	AP (mm)	Young	+8.71/-7.67
		Older	+4.66/-7.17
	IE (deg)	Young	+10.92/-7.97
		Older	+4.09/-4.44
	VV (deg)	Young	+7.81/-7.83
		Older	+5.24/-9.02
F1	AP (mm)	Young	+10.16/-7.39
		Older	+5.12/-5.49
	IE (deg)	Young	+13.30/-8.10
		Older	+3.54/-4.41
	VV (deg)	Young	+8.76/-15.35
		Older	+5.24/-8.10
F3	AP (mm)	Young	+11.78/-6.30
		Older	+5.42/-8.35
	IE (deg)	Young	+25.63/-5.89
		Older	+3.89/-5.45
	VV (deg)	Young	+10.07/-14.79
		Older	+8.46/-11.80
TO	AP (mm)	Young	+11.02/-10.05
		Older	+5.95/-8.37
	IE (deg)	Young	+16.83/-11.78
		Older	+7.72/-8.11
	VV (deg)	Young	+9.08/-11.65
		Older	+11.08/-13.80

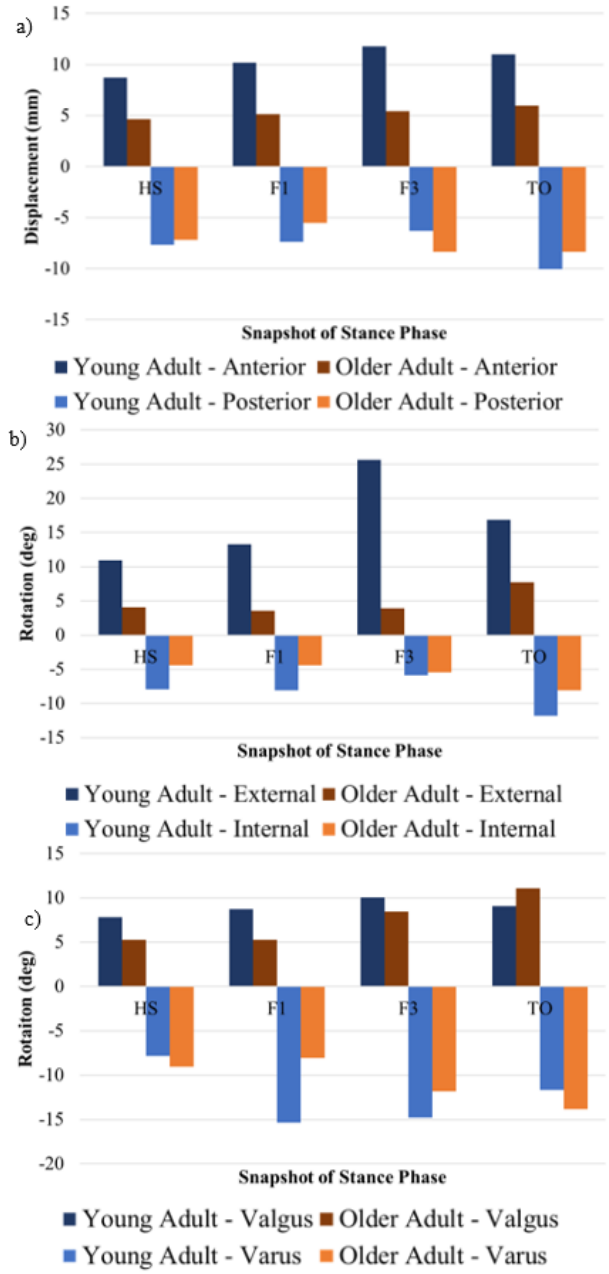

Figure 3.4: Displacements and rotations resulting from applied laxity loads and torques for a young (blue) and an older (orange) adult [HS: Heel Strike, F1: 1st Loading Peak, F3: 2nd Loading Peak, TO: Toe Off]. a) anterior-posterior displacement, b) external-internal rotation, and c) valgus-varus rotation.

differences observed here for the first and second loading peaks may mask age and sex effects since there were significant differences between ages for F1 and significant sex differences for F3 and these preliminary results only include one young and one older adult of opposite sexes. Greater joint motion observed for the older adult during the posterior (at the second loading peak) and varus (at heel strike and toe off) laxity tests may be suggestive reduced stability during these time points during stance.

Generic ligament properties were used for both participants. Changes in material properties due to aging may be present in the experimental trials but is not captured in the current finite element model. Future work will incorporate a ligament tuning process to assess whether there are age-related changes in ligamentous tissue properties.

CHAPTER 4:

CONCLUSIONS

4.1 Summary

Current literature lacks a synthesis of kinematics, kinetics, and muscle activity for activities of daily life, how these metrics of neuromechanics and whole-body function translate to the joint-level, and quantification of how strategies of musculoskeletal adaptation to challenging external conditions change with age. Consequently, the research of this thesis aimed to (Aim 1) evaluate musculoskeletal adaptation for gait on various challenging surfaces and (Aim 2) develop subject-specific finite element computational models for use in estimating joint-level adaptation and stability.

In order to address Aim 1, neuromechanical data were collected from twenty participants, ten older (5 male) and ten young (5 male). Inverse kinematics from experimental marker coordinates collected using motion capture were used to estimate joint angles. Vertical loading patterns and breaking and propulsive impulses were extracted from force plate data. Muscle activation and co-contraction strategies were assessed from lower limb electrodes. Combining these data for gait on normal, uneven, and slick surfaces, musculoskeletal adaptation strategies were identified and compared across surfaces, ages, and sexes.

Addressing Aim 2, a pipeline was developed to create subject-specific finite ele-

ment models combining experimental data, rigid-body musculoskeletal models, participant MRI geometry, and scaled musculature and tibiofemoral ligaments. This pipeline was applied to two participants drawn from the experimental cohort to demonstrate the feasibility to apply to these models the estimation of joint-level differences in a novel metric for functional, dynamic knee stability.

4.2 Limitations

Both aims of this research were dependent on the accuracy of the kinematics describing the motion of the experimental trials. This accuracy is dependent on both the data collection and OpenSim processes. During experimental motion capture data collection, markers placed on or over soft tissue, such as the thigh and greater trochanter, result in greater movement artifact and reduced accuracy (Cappozzo *et al.*, 1996). Therefore, these types of markers were considered calibration markers, weighting the confidence in the location of the marker lower, during processing in Visual3D and OpenSim. In order to reduce marker placement errors, the same, single researcher placed the markers for all but two data collection sessions. The process of scaling the generic OpenSim geometry for the rigid body model improves the quality and accuracy of the predicted joint kinematics; however, the OpenSim model does not include subject-specific soft tissues in the tibiofemoral joint, reducing the accuracy of predictions for non-sagittal plane kinematics. This limitation is addressed by combining the bones from the OpenSim model with subject-specific MRI geometry and allowing contact mechanics to drive the other degrees of freedom. However, in computational simulations there are always simplifications and assumptions made in the model development. In particular, generic ligament material properties were assumed during the dynamic laxity simulations. The tuning of these parameters will be the

focus of future research. Another limitation in the finite element model development is the process for generating subject-specific muscle activations. The current method of finding a scaling ratio from dynamometer tests may not be the most accurate estimation of muscle forces due to limited geometry detail in OpenSim and the detail available from the output of the dynamometer versus which muscles are modeled in OpenSim (i.e. lumped "quadriceps" for knee extension torque in the Humac activities but separate vastus and rectus femoris muscles in OpenSim). Therefore, future research will include proportional-integral feedback control for adjusting muscle forces to match flexion profiles.

4.3 Future Work

In order to improve the accuracy and capability to predict and investigate subject-specific adaptation strategies, there are a few improvements that would be beneficial and will be the focus of future work. Subject-specific ligament properties (stiffness and reference strain) will be calibrated according to the method used by Harris *et al.* at the University of Denver. This research group performed paired passive knee laxity experimental tests and finite-element simulations, calibrating the finite-element ligament properties to match experimental kinematics and literature ligament engagement behavior (Harris *et al.*, 2016). This method will be replicated by applying anterior-posterior force and internal-external and varus-valgus torques to subject-specific geometry aligned in the scan space according to Section 3.3. Ligament stiffness and reference strain for each modelled ligament bundle (Table 3.1) will be adjusted such that resulting kinematics from the finite element model are within the bounds of the published experimental and computational results. Subject-specific or age-specific ligament parameters will be determined from these laxity tuning simulations.

Additionally, proportional-integral feedback control will be implemented in the subject-specific 3D finite element model from Section 3.4 adjusting muscle force amplitudes to match knee joint kinematic profiles. This framework will also enable probabilistic investigations into the effect changing muscle forces has on stability in order to potentially inform targeted muscle training programs.

REFERENCES

Alcock, Lisa, Galna, Brook, Lord, Sue, & Rochester, Lynn. 2016. Characterisation of foot clearance during gait in people with early Parkinson's disease: Deficits associated with a dual task. *Journal of Biomechanics*, **49**(9), 2763–2769.

Allin, Leigh J., Wu, Xuefang, Nussbaum, Maury A., & Madigan, Michael L. 2016. Falls resulting from a laboratory-induced slip occur at a higher rate among individuals who are obese. *Journal of Biomechanics*, **49**(3), 678–683.

Ambrose, Anne Felicia, Paul, Geet, & Hausdorff, Jeffrey M. 2013. Risk factors for falls among older adults: A review of the literature. *Maturitas*, **75**(5), 51–61.

Arnold, Edith M., Ward, Samuel R., Lieber, Richard L., & Delp, Scott L. 2010. A model of the lower limb for analysis of human movement. *Annals of Biomedical Engineering*, **38**(2), 269–279.

Athwal, K. K., Milner, P. E., Bellier, G., & Amis, Andrew A. 2019. Posterior capsular release is a biomechanically safe procedure to perform in total knee arthroplasty. *Knee Surgery, Sports Traumatology, Arthroscopy*, **27**(5), 1587–1594.

Ball, S., Stephen, J. M., El-Daou, H., Williams, A., & Amis, Andrew A. 2020. The medial ligaments and the ACL restrain anteromedial laxity of the knee. *Knee Surgery, Sports Traumatology, Arthroscopy*, **28**(12), 3700–3708.

Begalle, Rebecca L., DiStefano, Lindsay J., Blackburn, Troy, & Padua, Darin A. 2012. Quadriceps and hamstrings coactivation during common therapeutic exercises. *Journal of Athletic Training*, **47**(8), 396–405.

Berry, Sarah D., & Miller, Ram R. 2008. Falls: Epidemiology, pathophysiology, and relationship to fracture. *Current Osteoporosis Reports*, **6**, 149–154.

Blankevoort, L., & Huiskes, R. 1991. Ligament-bone interaction in a three-dimensional model of the knee. *Journal of Biomechanical Engineering*, **113**, 263–269. Cited by several other papers for ligaments as springs and material properties.

Blankevoort, L., & Huiskes, R. 1996. Validation of a three-dimensional model of the knee. *Journal of Biomechanics*, **29**, 955–961.

C-motion. 2020a (10). *EMG Linear Envelope*.

C-motion. 2020b (8). *Functional Joints*.

Candotti, Cláudia Tarragô, Loss, Jefferson Fagundes, Bagatini, Daniel, Soares, Denise Paschoal, da Rocha, Everton Kruel, Álvaro Reischak de Oliveira, & Guimarães, Antônio Carlos Stringuini. 2009. Cocontraction and economy of triathletes and cyclists at different cadences during cycling motion. *Journal of Electromyography and Kinesiology*, **19**(10), 915–921.

Cappozzo, Aurelio, Catani, F., Leardini, A., Benedetti, M. G., & Croce, U. Della. 1996. Position and orientation in space of bones during movement: Experimental artefacts. *Clinical Biomechanics*, **11**(3), 90–100.

College, OpenStax. 2012. *College Physics: 5.1 Friction*. OpenStax.

Delp, Scott L., Anderson, Frank C., Arnold, Allison S., Loan, Peter, Habib, Ayman, John, Chand T., Guendelman, Eran, & Thelen, Darryl G. 2007. OpenSim: Open-source software to create and analyze dynamic simulations of movement. *IEEE Transactions on Biomedical Engineering*, **54**(11), 1940–1950.

Dixon, P. C., Schütte, K. H., Vanwanseele, B., Jacobs, J. V., Dennerlein, J. T., & Schiffman, J. M. 2018. Gait adaptations of older adults on an uneven brick surface can be predicted by age-related physiological changes in strength. *Gait and Posture*, **61**(3), 257–262.

Espy, D. D., Yang, F., Bhatt, T., & Pai, Y. C. 2010. Independent influence of gait speed and step length on stability and fall risk. *Gait and Posture*, **32**(7), 378–382.

Grabiner, Penny C., Biswas, S. Tina, & Grabiner, Mark D. 2001. Age-related changes in spatial and temporal gait variables. *Archives of Physical Medicine and Rehabilitation*, **82**, 31–35.

Grood, E. S., & Suntay, W. J. 1983. A joint coordinate system for the clinical description of three-dimensional motions: Application to the knee. *Journal of Biomechanical Engineering*, **105**, 136–144.

Hahn, Michael E., Lee, Heng Ju, & Chou, Li Shan. 2005. Increased muscular challenge in older adults during obstructed gait. *Gait and Posture*, **22**(12), 356–361.

Hallal, Camilla Zamfolini, Marques, Nise Ribeiro, Spinoso, Deborah Hebling, Vieira, Edgar Ramos, & Gonçalves, Mauro. 2013. Electromyographic patterns of lower limb muscles during apprehensive gait in younger and older female adults. *Journal of Electromyography and Kinesiology*, **23**(10), 1145–1149.

Harris, Michael D., Cyr, Adam J., Ali, Azhar A., Fitzpatrick, Clare K., Rullkoetter, Paul J., Maletsky, Lorin P., & Shelburne, Kevin B. 2016. A Combined Experimental and Computational Approach to Subject-Specific Analysis of Knee Joint Laxity. *Journal of Biomechanical Engineering*, **138**(8), 0810041.

HCUPnet. 2012. *Healthcare Cost and Utilization Project*.

Hermens, Hermie J., Freriks, Bart, Disselhorst-Klug, Catherine, & Rau, Günter. 2000. Development of recommendations for SEMG sensors and sensor placement procedures. *Journal of Electromyography and Kinesiology*, **10**(10), 361–374.

Hinman, Rana S., Bennell, Kim L., Metcalf, Ben R., & Crossley, Kay M. 2002. Delayed onset of quadriceps activity and altered knee joint kinematics during stair stepping in individuals with knee osteoarthritis. *Archives of Physical Medicine and Rehabilitation*, **83**, 1080–1086.

Homer, Mark L., Palmer, Nathan P., Fox, Kathe P., Armstrong, Joanne, & Mandl, Kenneth D. 2017. Predicting Falls in People Aged 65 Years and Older from Insurance Claims. *American Journal of Medicine*, **130**(6), 744.e17–744.e23.

Lee, Hwang Jae, Chang, Won Hyuk, Choi, Byung Ok, Ryu, Gyu Ha, & Kim, Yun Hee. 2017. Age-related differences in muscle co-activation during locomotion and their relationship with gait speed: a pilot study. *BMC Geriatrics*, **17**(1), 1–8.

Li, G., Gil, J., Kanamori, A., & Woo, S. L.Y. 1999. A validated three-dimensional computational model of a human knee joint. *Journal of Biomechanical Engineering*, **121**, 657–662.

Milholland, Adelle. 2019 (12). *Effect of Corrective Surgery on Lower Limb Mechanics in Patients with Crouch Gait.* M.Phil. thesis, Boise State University.

Moreland, Briana, Kakara, Ramakrishna, & Henry, Ankita. 2020. Trends in Nonfatal Falls and Fall-Related Injuries Among Adults Aged ≥65 Years — United States, 2012–2018. *MMWR. Morbidity and Mortality Weekly Report*, **69**(7), 875–881.

Nevitt, Michael C., Tolstykh, Irina, Shakoor, Najia, Nguyen, Uyen Sa D.T., Segal, Neil A., Lewis, Cora, & Felson, David T. 2016. Symptoms of Knee Instability as Risk Factors for Recurrent Falls. *Arthritis Care and Research*, **68**(8), 1089–1097.

Owings, Tammy M., & Grabiner, Mark D. 2004. Variability of step kinematics in young and older adults. *Gait and Posture*, **20**(8), 26–29.

Pandy, Marcus G., Sasaki, Kotara, & Kim, Seonfil. 1997. A three-dimensional musculoskeletal model of the human knee joint. Part 1: Theoretical construction. *Computer Methods in Biomechanics and Biomedical Engineering*, **1**, 87–108.

R Core Team. 2020. *R: A Language and Environment for Statistical Computing.* R Foundation for Statistical Computing, Vienna, Austria. 4.0.3.

Rodriguez-Vila, B., Sánchez-González, P., Oropesa, I., Gomez, E. J., & Pierce, D. M. 2017. Automated hexahedral meshing of knee cartilage structures–application to data from the osteoarthritis initiative. *Computer Methods in Biomechanics and Biomedical Engineering*, **20**(10), 1543–1553.

Rubenstein, Laurence Z., & Josephson, Karen R. 2002. The epidemiology of falls and syncope. *Clinics in Geriatric Medicine*, **18**(5), 141–158.

Saywell, Nicola, Taylor, Denise, & Boocock, Mark. 2012. During step descent, older adults exhibit decreased knee range of motion and increased vastus lateralis muscle activity. *Gait and Posture*, **36**(7), 490–494.

Schmitz, Anne, Silder, Amy, Heiderscheit, Bryan, Mahoney, Jane, & Thelen, Darryl G. 2009. Differences in lower-extremity muscular activation during walking between healthy older and young adults. *Journal of Electromyography and Kinesiology*, **19**(12), 1085–1091.

Schnell, Scott, Friedman, Susan M., Mendelson, Daniel A., Bingham, Karilee W., & Kates, Stephen L. 2010. The 1-Year Mortality of Patients Treated in a Hip Fracture Program for Elders. *Geriatric Orthopaedic Surgery & Rehabilitation*, **1**, 6–14.

Schrager, Matthew A., Kelly, Valerie E., Price, Robert, Ferrucci, Luigi, & Shumway-Cook, Anne. 2008. The effects of age on medio-lateral stability during normal and narrow base walking. *Gait and Posture*, **28**, 466–471.

Schwartz, Michael H., & Rozumalski, Adam. 2005. A new method for estimating joint parameters from motion data. *Journal of Biomechanics*, **38**(1), 107–116.

Thies, Sibylle B., Richardson, James K., & Ashton-Miller, James A. 2005. Effects of surface irregularity and lighting on step variability during gait: A study in healthy young and older women. *Gait and Posture*, **22**.

Winter, David A. 2009. *Biomechanics and Motor Control of Human Movement*. John Wiley & Sons, Ltd.

Worsley, Peter, Stokes, Maria, & Taylor, Mark. 2011. Predicted knee kinematics

and kinetics during functional activities using motion capture and musculoskeletal modelling in healthy older people. *Gait and Posture*, **33**(2), 268–273.

APPENDIX A:

PARTICIPANT DEMOGRAPHICS

Table A.1: Represented ethnicities

	Young Adults ($n = 10$)	Older Adults ($n = 10$)
White/Caucasian	7	8
Hispanic/Latino	2	0
African-American	1	1
Asian-American	0	1

Participants of diverse height and weight, and representative of diverse ethnicities, were matched across cohorts according to gender, height, and BMI. Ethnicities represented in this study are as seen in Table A.1. Referenced in Section 2.2.

APPENDIX B:

HUMAC NORM DYNAMOMETER

Table B.1: Humac Norm dynamometer strength results (young vs older adults)

	Young Adults ($n = 10$)	Older Adults ($n = 10$)	p-value
Knee Flexion (N-m)	116.5 ± 57.6	71.7 ± 26.6	**<0.05***
Knee Extension (N-m)	203.4 ± 102.1	120.9 ± 56.1	**<0.05***
Hip Flexion (N-m)	94.3 ± 39.9	83.7 ± 39.1	p=0.56
Hip Extension (N-m)	109.1 ± 49.2	102.0 ± 36.9	p=0.72
Ankle Dorsiflexion (N-m)	36.5 ± 12.6	90.3 ± 47.1	**<0.05***
Ankle Plantarflexion (N-m)	90.3 ± 47.1	38.8 ± 15.8	**<0.01***

*p<0.05. Significant differences between young and older adults.

Table B.2: Humac Norm dynamometer strength results (female vs male)

	Females ($n = 10$)	Males ($n = 10$)	p-value
Knee Flexion (N-m)	70.6 ± 31.5	117.6 ± 54.0	**<0.05***
Knee Extension (N-m)	113.8 ± 57.4	210.5 ± 94.1	**<0.05***
Hip Flexion (N-m)	74.9 ± 22.2	103.1 ± 47.4	p=0.11
Hip Extension (N-m)	90.4 ± 27.6	120.7 ± 50.4	p=0.11
Ankle Dorsiflexion (N-m)	25.7 ± 7.2	33.3 ± 16.4	p=0.20
Ankle Plantarflexion (N-m)	49.4 ± 18.7	79.7 ± 55.5	p=0.12

*p<0.05. Significant differences between females and males.

Strength and strength differences from the Humac Norm dynamometer (Tables B.1 and B.2). Referenced in Sections 2.2 and 3.5.